VIBRATION AND THERMAL ANALYSIS AND OPTIMUM DESIGN OF VISCOELASTIC SANDWICH BEAM

Jasrobin Singh Grewal

A thesis

In the Department of

Mechanical and Industrial Engineering

Presented in Partial Fulfillment of the Requirements

For the Degree of Master of Applied Science

at

Concordia University

Montreal, Quebec, Canada

September 2011

i

CONCORDIA UNIVERSITY

SCHOOL OF GRADUATE STUDIES

This is to certify that the Thesis prepared,

By: **Jasrobin Singh Grewal**

Entitled: **"Vibration and Thermal Analysis and Optimum Design of Viscoelastic Sandwich Beam"**

And submitted in partial fulfillment of the requirements for the Degree of

<u>Master of Applied Science (Mechanical Engineering)</u>

Complies with the regulations of this University and meets the accepted standards with respect to originality and quality.

Signed by the Final Examining Committee:

_____ Chair

Dr. I. Hassan

_____ Examiner

Dr. R. Bhat

_____ Examiner External

Dr. S. Li

_____ Co-Supervisor

Dr. R. Sedaghati

_____ Co-Supervisor

Dr. E. Esmailzadeh

Approved by: _____
                  Dr. A.K.W. Ahmed, MASc Program Director
                  Department of Mechanical and Industrial Enginering

                  _____
                  Dean Robin Drew
                  Faculty of Engineering & Computer Science

Date: _____

ii

Abstract

Sandwich beam structures have many applications in various fields of engineering including especially in aerospace and transportation industries. Using the viscoelastic material as the core layer in these structures, one could include significant amount of damping with minimum impact on the total mass of the structure. In the current study, vibration damping analyses of the sandwich beam structure using the finite element formulations are presented. These formulations are developed based on the linear and non-linear displacement fields in the viscoelastic core layer. Results obtained from the present study were compared with those reported in literature and it is shown that the non linear displacement field exhibits more accurate damping response than the linear model. Parametric sensitivity analysis has been carried out to show the damping behavior of partially treated sandwich beam under different configuration. Genetic algorithm is utilized in finding the optimum configuration to achieve the highest damping. Results show that for damping behavior of beam with the clamped-clamped boundary condition, the partially treated beam structure is more effective than the fully treated one. Also the effect of the heat dissipation in the damping layer of the beam on the damping performance of the viscoelastic material is investigated under the steady-state harmonic excitation. The generated heat has been taken into the consideration by implementing the finite difference formulation based on the irregular grids. Results obtained clearly indicate that the temperature gradient developed in the structure and hence the amplitude of the response increases after every cycle.

This work is dedicated to my parents,

Harpal Singh and Supinder Kaur

And to my wife

Gurpal Kaur

And to my daughter

Samayra

Acknowledgements

Table of Contents

List of Figures

List of Tables

CHAPTER 1

1   INTRODUCTION AND LITERATURE SURVEY

1.1   Motivation and Objectives

Vibration directly influences the performance and life of engineering structures, and invariably, damping in the structures influenced its vibration behavior. Various types of damping mechanisms have been developed over time to control the undesired vibration of structures. Damping basically refers to the extraction of the mechanical energy from a vibrating system, mainly by converting the mechanical energy into heat energy by means of some dissipation mechanism. Although all materials exhibit certain amount of internal structural damping, most of the time it is not substantially effective to suppress the vibration around resonant frequencies. However, by bringing these materials in contact with the highly damped and dynamically stiff material, it is possible to control the vibration. Viscoelastic materials are one such type that are capable of storing strain energy when they are deformed, while dissipating a portion of their energy through hysteresis. Viscoelastic damping property is exhibited by the large variety of polymeric materials, ranging from natural/synthetic rubbers to various thermoplastic/thermoset materials used in different industries. Due to large molecular order and having tangled molecules, polymers display rheological behavior intermediate between a crystalline solid and a simple fluid. Of great importance is the dependency of both the stiffness and damping parameters on the frequency and temperature. These viscoelastic materials offer a wide range of

possibilities for developing desire level of damping, provided the designer has thoroughly comprehended their mechanical behavior. The mechanical energy is dissipated via cyclic shear and normal deformation of the viscoelastic material. There are broadly two ways to apply viscoelastic material on structure: free layer damping treatment, here mainly it goes under normal deformation as the structure bends, and by incorporating a constrained layer over the free layer treatment, which will enhance the shear strain in the viscoelastic material, also known as constrained layer damping treatment.

The frequency and temperature dependencies of the passive damping mechanism must be taken into account during the design. To achieve a proper damping value, two conditions must be fulfilled: 1. significant strain energy must be engaged into the applied viscoelastic material for all modes of interest, so that the energy in the viscoelastic material can be dissipated in the form of heat energy, 2. the heat generated must be conducted away either from the viscoelastic material through structure or directly to environment because the damping properties of viscoelastic material are very sensitive to temperature.

To achieve both conditions, an accurate mathematical model either analytical or numerical model of the damped structure is to be developed. The model must be numerically stable to accommodate the small changes in the design and can be easily integrated with the optimization algorithm to perform multiple parameter optimizations. Considering above, the objectives of this research could be specified as:

1. To develop a finite element model of a viscoelastic sandwich beam for symmetrical/unsymmetrical constrained layer and partially treated layer configurations under different boundary conditions. The developed model should be validated against previously published theories and experiments. It should also be numerically stable, computationally efficient and the results comparable to classical models.

2. To digitize the given mechanical properties of the viscoelastic material, being the modulus and loss factor as function of temperature and frequency from the available nomogram and efficiently incorporate them into the developed finite element model.

3. To study the effect of the thickness of the viscoelastic layer on the damping performance of the system.

4. To optimize the location and area of the partially treated damping layers for a viscoelastic sandwich beam in order to maximize the damping performance under given constraints.

5. To develop a central finite difference model, for evaluating the temperature gradient developed in all layers due to the internal heat generated.

1.2 Damping treatment design

There are different ways to apply viscoelastic material to structure and design viscoelastic sandwich structure which includes: (i) the full treatment of unconstrained viscoelastic material layer, (ii) the full treatment of constrained viscoelastic material layer and (iii) the partial treatment of viscoelastic layers.

1.2.1   Free (unconstrained) Layer Damping (FLD)

FLD treatment is unconstrained layer construction with viscoelastic layer bonded using an adhesive to one or both sides of a base layer. When the base layer is deflected in bending, the viscoelastic layer undergoes extension and compression in planes parallel to base layer. The hysteresis loop of the cyclic stress and strain dissipates the energy in the form of heat. The degree of damping is constrained by the thickness and weight limits.   Figure (1.1) illustrates portion of a structure treated with a free viscoelastic layer.

Figure 1.1 Free Layer Damping

The vibration analysis of a beam with a viscoelastic layer was first conducted by (Kerwin, 1959). The viscoelastic material's characteristic was modeled using complex modulus approach. It was found that the system loss factor in a free layer treatment increases with thickness, storage modulus and loss factor of the viscoelastic material layer.

1.2.2   Constrained Layer Damping (CLD).

The constrained layer damping, shown in Figure (1.2) consists of an additional top layer on the free layer damping treatment.
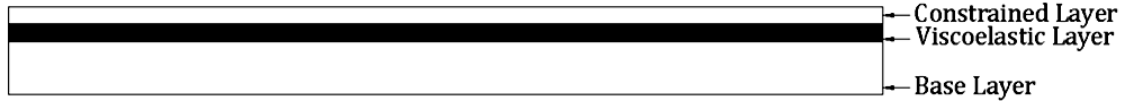
Figure 1.2 Constrained Layer Damping

 When the base structure undergoes bending vibration, the viscoelastic material is forced to deform in shear because of the upper stiff layer. The constrained layer damping is more efficient than free layer damping because the core layer can store more strain energy and therefore dissipates more energy. The symmetric design in which base layer and top constraining layer is of same thickness is most effective configuration as it maximizes the shear strain in the core layer. The CLD can be extended to multiple constrained layers, which is very effective for obtaining damping over wide temperature and frequency ranges. Also to reduce the weight of structure, the constrained layers are implemented in patches as partial treatment shown in Figure (1.3).

Figure 1.3 Partial Constrained Layer Damping

1.3   State-of-the-art

1.3.1   Viscoelastic Material

Concepts of passive damping and methods to determine damping are elegantly presented in the book (Nashif, et al., 1985). The book thoroughly discusses the viscoelastic material behavior and typical properties and modeling of structural response of damped systems. Nashif, Jones and Henderson (Nashif, et al., 1985) represented viscoelastic material using a complex modulus in the frequency

domain. The complex modulus model is motivated by observing the relation between applied sinusoidal stress and sinusoidal strain developed in viscoelastic material. When the single degree of freedom system is excited by a harmonic force of constant amplitude, the steady state response of the system can be used to determine the damping through the amplitude of response at resonance, Half-power Bandwidth, Nyquist diagram, hysteresis loops, and dynamic stiffness. Typical damping properties of viscoelastic material depends on various factors like frequency, temperature, dynamic strain, static preload, and other environmental factors like aging, pressure, oil exposures, though the effects of environment factors can be observed only under extreme conditions. Factors that influence the behavior of viscoelastic material predominately are frequency and temperature. The temperature nomogram was developed by the Jones (Jones, 1978) to represent elastic modulus and loss factor of material in a master curves that are convenient for practical applications. Several of these master curves are shown in (Jones, 2001) and appendices of (Nashif, et al., 1985).

Damping models for the viscoelastic materials must capture the frequency dependent complex modulus in the frequency domain and also exhibit the creep and relaxation properties in the time domain. Shaw and MacKnight (Shaw, et al., 2005) reviewed damping models including the Maxwell, the Kelvin, and the Zener model (Zener, 1948). These models have some drawbacks and cannot capture the real behavior of the viscoelastic materials. The creep function predicted by the Maxwell model does not converge to steady state value but keep on increasing with time and the relaxation function predicted by the Voigt model keeps constant throughout the

time. The Zener model can predict both creep and relaxation functions well but when one compare the complex modulus to experimental data; the variation with frequency is much more rapid. Generalized standard models consist of large number of elements combining both Maxwell and Voigt elements which may greatly improve the creep and relaxation functions; however, it significantly increases the mathematical complexity. However, modeling viscoelastic material has been simplified with respect to frequency domain, using the fractional derivate model approach. Bagley and Torvik (Bagley, et al., 1983) have improved the damping model by reducing the parameters considerably, as required by the generalized standard model. The advantage of the fractional derivates models is not only their capabilities for representing dynamic behavior, but they are simple enough for engineering calculation. Golla, McTavish and Hughes (GHM) model (Golla, et al., 1985; McTavish, et al., 1993) represent a viscoelastic material by introducing internal variable (Auxiliary dissipation coordinates) to account for viscoelastic relaxation and, thus damping. They represented shear modulus function in the Laplace domain using series of mini-oscillatory. Christensen (Christensen, 1971) developed a time domain model using a relaxation function which can be transformed into frequency domain, thus obtaining a complex modulus. The properties of the relaxation function were based on the physical principles. But it is very difficult to transform such relaxation function to capture a complex modulus in the frequency domain. There are other models such as Augmenting Thermodynamics Fields (ATF) (Lesiutre, et al., 1990) and Anelastic Displacement

Fields (ADF) (Lesieutre, et al., 1995) method. These models can also be used to account for the frequency dependent complex modulus of viscoelastic material.

1.3.2 Sandwich Beams

For damping treatment with viscoelastic materials Grootenhuis (Grootenhuis, 1970) summarized prior research. There are mainly two types of surface damping treatment: unconstrained and constrained. In the unconstrained layer treatment, a layer of viscoelastic material is applied with adhesive to the surface of structure. The energy is dissipated by the cyclic tensile and compressive strain when structure is in bending motion. In the case of constrained layer treatment, a stiff layer is added with adhesive to the top surface of viscoelastic layer so that the viscoelastic layer is sandwiched between the main base structure and elastic top layer. In this case, when the sandwich structure undergoes bending motion, the constrained layer causes significant shear deformation in the viscoelastic layer. The constrained layer damping treatment is more efficient because the viscoelastic materials dissipate energy mainly by the shear deformation and the constrained layer augments the magnitude of shear deformation significantly.

Kerwin (Kerwin, 1959) has presented the first analysis of the simply supported sandwich beam using a complex modulus to represent the viscoelastic core. He stated that the energy dissipation mechanism in the constrained viscoelastic core is because of shearing. His model predicted attenuation of a traveling wave on a simply supported and an infinite long beam (neglecting the end effects), vibrating at a natural frequency. Di Taranto (DiTaranto, 1965) extended Kerwin's work using

same basic assumption and derived a sixth-order, homogeneous equation in terms of the longitudinal displacement for free vibration of a constrained layer beam. Damping of the beam is considered due to complex shear modulus of the viscoelastic layer. The sixth-order, homogeneous equation yields natural frequency and associated loss factor subjected to boundary conditions. Assuming that the shear strains in the base layer and constrained layer, longitudinal stresses in the core, and the transverse strains in all three layers are negligible, Mead and Markus (Mead, et al., 1969) proposed a sixth-order differential equation of motion in terms of the transverse displacement for three layer sandwich beam with viscoelastic as core layer. They also found expression for transverse displacement for different boundary conditions of the beam. Yan and Dowell (Yan, et al., 1972) proposed a fourth-order equation of motion for beams and plates. The top and bottom layer's shear deformation, and longitudinal and rotary inertia were considered to derive sixth-order differential equations which are then ignored so as to acquire a simplified fourth-order differential equation. Mead (Mead, 1983) examined the preceding theories of Yan and Dowell, Di Taranto, and Mead and Markus and concluded that most authors have made the same basic assumptions including: (i) the linear viscoelastic core carried only shear stress and had complex shear modulus; (ii) Top and bottom layers were elastic and isotropic going under shear deformation normal to the surface; (iii) The inertial forces of transverse flexural motion were dominant; (iv) Transverse displacement at all points on area normal to axis was the same; (v) No slip occurred at the interface of the core and top and bottom layers (perfect bonding). He also concluded that the Di Taranto and Mead

and Markus equations yield accurate results provided the flexural wavelength is greater than about four times the top and bottom layers thicknesses. The Yan and Dowel equations yield reliable values at much longer wavelengths or when the core layer is very thick (Mead, 1983). Kung and Singh (Kung, et al., 1999) proposed an analytical method considering, longitudinal, rotational and shear deformations in all layers of sandwich beams with constrained layer damping patches. The results for single patch were verified by comparing with reported results by Lall, Asnani and Nakra (Lall, et al., 1988). Bai and Sun (Bai, et al., 1995) eliminate the assumptions that there is perfect interface between sandwich layers and also that the top and bottom layers goes under constant transverse displacement. The core is modeled as frequency dependent viscoelastic materials and top and bottom layers considered as elastic beams. The Bai and Sun theory incorporate a shear deformation by using a second order displacement field, which allows core to deform in a non-linear manner through the thickness. Later Baber, Maddox and Orozco (Baber, et al., 1998) have presented a finite element model that is derived using the Bai and Sun assumption of nonlinear displacement field in the core but neglecting the slippage between the layers and considering classic theory of beam in top and base layers. The presented model contains 12 degree of freedom per element.

One of the objectives of the present study is to compare the results of assuming linear displacement fields in core or nonlinear displacement fields. Finite element model by (Baber, et al., 1998) is modified for the nonlinear displacement field, and for linear displacement field in core a separate Finite element model is developed.

1.4   Models to characterize the behavior of Viscoelastic Material

The damping phenomenon in viscoelastic material arises from the relaxation and recovery of the polymer network after it has been deformed. As the name viscoelastic implies, it shows characteristics of both viscous fluid and elastic solid material. In the viscous fluid the mechanical energy is dissipated in the form of heat and in elastic solid the energy is stored in the form of strain energy. This combination of properties makes the viscoelastic material to behave uniquely, such that in addition to undergoing instantaneous strain it also undergoes creep after the application of constant sudden load. Alternatively, one can say that the force required for maintaining constant strain will decrease over the period of time. In order to develop constitutive relation between stress and strain, one need to do transient or dynamic analysis. Under the sinusoidal strain loading of frequency ω, experimental results (Shaw, et al., 2005) clearly show that the stress and strain of a linear viscoelastic material oscillate at the same frequency but with a phase difference of δ.
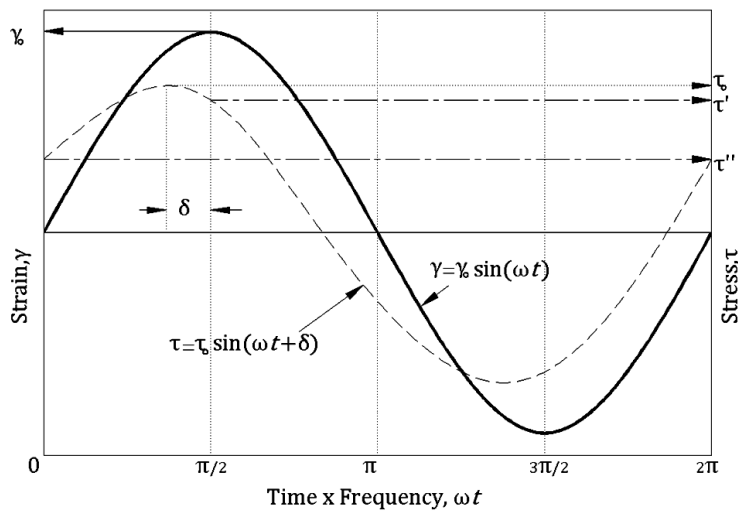
Figure 1.4 Stress and Strain under sinusoidal strain loading (Shaw, et al., 2005)

As shown in Figure (1.4), the strain rate has maximum value as it passes through zero and corresponding stress τ'' is the stress as if the sample would behave purely as in a viscous. Alternatively as the strain rate becomes zero when strain reaches its maximum value, corresponding stress τ' is the stress as if the sample would be purely elastic.

1.4.1   Constitutive Equation of Viscoelastic Material

Boltzmann superposition principle helps greatly to develop the constitutive equation for viscoelastic material. It states that each loading step makes independent influence on loading history and total strain of sample is linear summation of all the strains. In a Creep test where shear stress τ_o is applied instantaneously at time zero and strain is measured over the time, the resulting shear creep compliance can be written as

$$J(t) = \frac{\gamma(t)}{\tau_o} \tag{1.1}$$

This can also be written as

$$\gamma(t) = \tau_o J(t) \tag{1.2}$$

In general the stress τ_o can be applied at any arbitrary time r_1. Then the equation (1.2) takes the form of

$$\gamma(t) = \tau_1 J(t - r_1) \qquad\qquad t \geq r_1$$
$$\tag{1.3}$$
$$\gamma(t) = 0 \qquad\qquad t < r_1$$

If one consider both loading steps of stress at time equal to zero and t_1. After applying Boltzmann superposition principle as defined above, one can write:

$$\gamma(t) = \tau_o J(t) + \tau_1 J(t - r_1) \tag{1.4}$$

For more general loading one can consider number of discrete stress increments $\tau_1, \tau_2, \tau_3, \ldots \tau_n$ applied at time $t = r_1, r_2, r_3, \ldots r_n$ and then one can extend the Eq. (1.4) into the following form:

$$\gamma(t) = \sum_{i=1}^{n} \tau_i J(t - r_i) \tag{1.5}$$

Instead of discrete increment of stress τ_i considering a continuous stress $\tau(r)$, the increment of stress is just derivative of $\tau(r)$ times the increment of time dr. One can then easily replace the summation in Eq. (1.5) by the integration as:

$$\gamma(t) = \int_{-\infty}^{t} \frac{\partial \tau(r)}{\partial r} J(t - r) dr \tag{1.6}$$

Lower limit of integration is $-\infty$, so that influence of complete loading history can be considered for observed strain. Using the same analogy, one can derive an expression of stress $\tau(t)$ for a sample which has continuous strain history of $\gamma(t)$.

$$\tau(t) = \int_{-\infty}^{t} \frac{\partial \gamma(r)}{\partial r} G(t - r) dr \tag{1.7}$$

By setting $(t-r)$ equal to new variable b and taking care of new limits, Eq. (1.7) becomes

$$\tau(t) = -\int_0^\infty \frac{\partial \gamma(t-b)}{\partial b} G(b) db \qquad (1.8)$$

Now under the application of harmonic shear strain at any time b, one can write:

$$\gamma(t-b) = \gamma_0 e^{i\omega(t-b)} \qquad (1.9)$$

Substituting the Eq. (1.9) into Eq. (1.8) and after the integration and simplification yields a complex modulus as:

$$G^* = G'(\omega) + i\,G''(\omega) \qquad (1.10)$$

here $G'(\omega)$ is the storage shear modulus and $G''(\omega)$ is the loss shear modulus. The loss factor $\eta(\omega)$ of a material can be defined as the non-dimensional quantity computed by dividing $G''(\omega)$ the loss shear modulus by $G'(\omega)$ the storage shear modulus as:

$$G^* = G'(\omega)\big(1 + i\eta(\omega)\big) \qquad (1.10a)$$

$$\eta(\omega) = \left(\frac{G''(\omega)}{G'(\omega)}\right) \qquad (1.10b)$$

The loss factor indicates the ratio of average energy dissipated from the viscoelastic material to the maximum strain energy stored under a harmonic force over the period of one cycle. A complex modulus that illustrates the steady state harmonic response of the viscoelastic material is also used to obtain the characteristics of the viscoelastic material. As discussed in the introduction, the mechanical properties of viscoelastic material depend not only on the frequency but also on the temperature, and so is the complex modulus. There are various procedures for determining the complex modulus of viscoelastic materials through experiments. The details of test

setup, specimen selection criteria and test procedures are described in (Nashif, et al., 1985) and (Jones, 2001). The important characteristics of damping materials are shown in a temperature nomogram. The concept of nomogram was developed by Jones (Jones, 1978) and is considered as a standard presentation of complex modulus data. The data for the nomogram of viscoelastic materials are provided by the manufacturers for a particular lot. The storage and loss factor of the material can be obtained from the nomogram.

1.4.2   Damping Models

To comprehend the effect of relaxation behavior of viscoelastic material and to represent it mathematically, the need of specific mechanical analog model arises. Simplest way to capture both elastic and relaxation nature of polymers is by developing a model consisting of both elastic solid and viscous fluid dashpot. Various models with different combinations of solid and viscous fluid dashpot have been developed and here in the following we will briefly discuss Maxwell, Voigt, Zener Models known as Standard Solid Models, Generalized standard model and Fractional derivate (FD) method (Bagley, et al., 1983). We will show that Maxwell and Voigt models are not able to replicate the complete behavior of viscoelastic structure but the improved generalized standard and Fractional derivate models comparatively capture the behavior. Further we will discuss some modern approaches like the Augmenting Thermodynamics Fields (ATF) (Lesiutre, et al., 1990) method, the Anelastic Displacement Field (ADF) (Lesieutre, et al., 1995) method and the Golla-Huges-McTavish (GHM) method (Golla, et al., 1985). The merits and demerits of these methods will also be discussed.

Before discussing these models, it may be better to briefly go over the constitutive equation for elastic solid and viscous fluid (Dashpot).

Elastic Solid:

Elastic spring in Figure (1.5) can easily replace for elastic solid. Here the linear spring constant is the modulus of elasticity. The relation between the elastic strain ε_e and elastic stress σ_e can then be described by the Hook's relation as:

Figure 1.5 Elastic Spring

$$\sigma_e = E\varepsilon_e \tag{1.11}$$

where E is Young's Modulus of elasticity.

Here stress and strain are independent of time.

Viscous Fluid Dashpot:

Viscosity is the dominant nature of fluids in viscous fluid dashpot as shown in Figure (1.6).
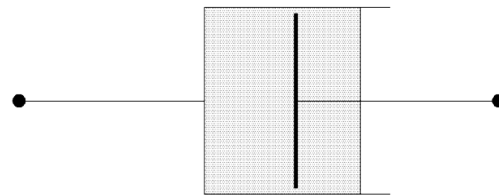
Figure 1.6 Viscous Dashpot

16

The constitutive equation of viscous fluid is governed by the Newtonian law of viscosity, which implies stress in fluid is linearly proportional to strain rate as:

$$\sigma_v = \mu \frac{d\varepsilon_v}{dt} \tag{1.12}$$

where, μ is known as coefficient of viscosity.

The ratio of μ to E is defined as relaxation time of element.

$$T_r = \frac{\mu}{E} \tag{1.13}$$

Maxwell Model:

In the Maxwell model elastic spring and dashpot are connected in series as shown in Figure (1.7) to approximate the mechanical response of viscoelastic material.
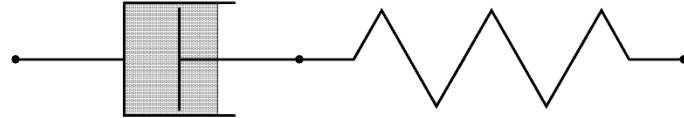
Figure 1.7 Schematic representation of Maxwell Model

If a stress σ is applied at one end of this model stresses in both spring σ_e and dashpot σ_v can be written as

$$\sigma = \sigma_e = \sigma_v \tag{1.14}$$

And total strain ε in the element is linear summation of strain in elastic spring ε_e and strain in viscous dashpot ε_v can be written as

$$\varepsilon = \varepsilon_e + \varepsilon_v \tag{1.15}$$

17

Differentiating the above Eq. (1.15) with respect to time and considering Eqs. (1.11), (1.12) and (1.14), one may write the governing differential equation for Maxwell model as:

$$\frac{d\varepsilon}{dt} = \frac{1}{E}\frac{d\sigma}{dt} + \frac{\sigma}{\mu}$$

(1.16)

This governing differential equation can be solved for three types of loading.

Under the Creep loading, the stress is suddenly applied to previously unstrained sample and maintained at constant value, and thus stress can be written as:

$$\sigma(t) = \sigma_o H(t)$$

(1.17)

where $H(t)$ is the Heavyside function and is defined as

$$H(t) = 1 \qquad for\, t > 0$$

$$H(t) = 0 \qquad for\, t < 0$$

Replacing the stress from Eq. (1.17) into the Eq. (1.16) and then integrating with respect to time yields:

$$\varepsilon(t) = \sigma_o\left(\frac{1}{E} + \frac{t}{\mu}\right)H(t)$$

(1.18)

$$\varepsilon(t) = \sigma_o D(t)$$

(1.19)

where $D(t)$ is creep compliance.

Alternatively, if strain is suddenly applied and maintained at a constant value, then $\frac{d\varepsilon}{dt}$ is zero, which makes the Eq. (1.16) to take a form of

18

$$\frac{1}{E}\frac{d\sigma}{dt}+\frac{\sigma}{\mu}=0 \tag{1.20}$$

This equation can easily be integrated from σ_o at time equals to zero to σ_t at time equals to t to have:

$$\ln\sigma_t=\ln\sigma_o\left(-\frac{tE}{\mu}\right) \tag{1.21}$$

Taking exponential from both sides of Eq. (1.21) and considering $\sigma_o=E\,\varepsilon_o$ yields:

$$\sigma_t=\varepsilon_o Ee^{-\frac{tE}{\mu}} \tag{1.22}$$

On the other hand, if the loading is harmonic in nature with frequency ω, the strain produced will also be harmonic with same frequency but with phase difference δ.

Harmonic stress can be represented as

$$\sigma_t=\sigma_o e^{i\omega t} \tag{1.23}$$

Here σ_o is amplitude of stress and ω is frequency (radian/s). Replacing the stress from Eq. (1.23) in Eq. (1.16) yields:

$$\frac{d\varepsilon}{dt}=\frac{\sigma_0}{E}i\omega e^{i\omega t}+\frac{\sigma_0}{\mu}e^{i\omega t} \tag{1.24}$$

Integrating the Eq. (1.21) with respect to time from time equals to t_1 to time equals to t_2 gives

$$\varepsilon(t_2)-\varepsilon(t_1)=\frac{\sigma_0}{E}(e^{i\omega t_2}-e^{i\omega t_1})+\frac{\sigma_0}{i\omega\mu}(e^{i\omega t_2}-e^{i\omega t_1}) \tag{1.25}$$

Rearranging one get

$$\frac{\varepsilon(t_2)-\varepsilon(t_1)}{\sigma(t_2)-\sigma(t_1)} = \left(\frac{1}{E}-i\,\frac{1}{\omega\mu}\right) \tag{1.26}$$

We can write

$$D^* = \left(\frac{1}{E}-i\,\frac{1}{\omega\mu}\right) \tag{1.27}$$

where D^* is the complex tensile compliance, from here we can easily calculate the E^*, the complex tensile modulus, as

$$E^* = \frac{1}{D^*} \tag{1.28}$$

$$E^* = E' + i\,E'' \tag{1.29}$$

$$E' = \frac{E\mu^2\omega^2}{E^2 + \mu^2\omega^2} \tag{1.30}$$

$$E'' = \frac{E^2\mu\omega}{E^2 + \mu^2\omega^2} \tag{1.31}$$

Voigt Model

In the Voigt model, the spring and dashpot are connected in parallel to each other as shown in Figure (1.8) which results into the equation for stress as:

$$\sigma = \sigma_e + \sigma_v \tag{1.32}$$

where, σ_e is the stress in the elastic spring and σ_v is the stress in the viscous dashpot.

Strain produced in the elastic spring ε_e and viscous dashpot ε_v is the same.

$$\varepsilon = \varepsilon_e = \varepsilon_v \tag{1.33}$$
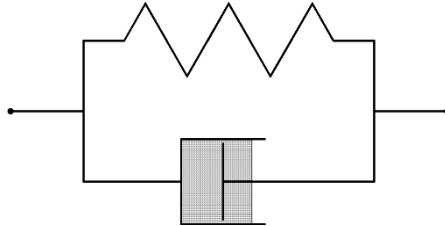
Figure 1.8 Schematic representation of Voigt Model

Using the stress and strain constitutive relation from Eq. (1.11) and Eq. (1.12) governing differential equation for Voigt model can be written as

$$\sigma = E\varepsilon + \mu \frac{d\varepsilon}{dt} \tag{1.34}$$

Under creep test, stress is suddenly applied and maintained at constant value as defined in Eq. (1.17), thus we can write:

$$\sigma_0 H(t) = E\varepsilon + \mu \frac{d\varepsilon}{dt} \tag{1.35}$$

Multiplying both side of Eq. (1.35) by $e^{\frac{Et}{\mu}}$ gives:

$$\sigma_0 e^{\frac{Et}{\mu}} H(t) = \mu \frac{d(e^{\frac{Et}{\mu}} \varepsilon)}{dt} \tag{1.36}$$

Integration both side of Eq. (1.36) with respect to time, we have:

$$\varepsilon(t) = \frac{\sigma_0}{E} \left(1 - e^{-\frac{Et}{\mu}} \right) H(t) \tag{1.37}$$

$$\varepsilon(t) = \frac{\sigma_0}{E} D^* \tag{1.38}$$

$$D^* = \left(1 - e^{-\frac{Et}{\mu}}\right) H(t) \tag{1.39}$$

D^* is known as Creep Compliance.

Alternatively, if strain is suddenly applied and maintained at a constant value which means $\dfrac{d\varepsilon}{dt}$ is zero, then Eq. (1.34) takes the following form as:

$$\sigma = E\varepsilon \tag{1.40}$$

Under the harmonic loading, taking the analogy as discussed previously for the Maxwell model, one can reach to $E^* = E' + i\,E''$ complex tensile modulus as:

$$E' = E \tag{1.41}$$

$$E'' = \omega\mu \tag{1.42}$$

Zener Model

In Zener model, two elastic springs are attached with a single dashpot in serial and parallel combination as shown in Figure (1.9). The constitutive equation for this model can be written as

$$\sigma + \alpha \frac{d\sigma}{dt} = E\varepsilon + \beta E \frac{d\varepsilon}{dt} \tag{1.43}$$
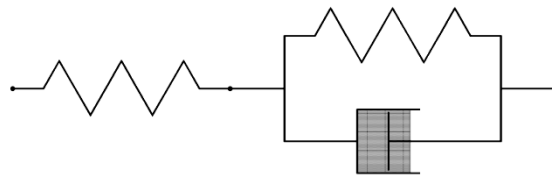
Figure 1.9 Schematic representation of Zener Model

The parameters α, β, E in Eq. (1.38) are defined here

$$\alpha = \frac{\mu}{E_1 + E_2} \tag{1.44}$$

$$\beta = \frac{\mu}{E_1} \tag{1.45}$$

$$E = \frac{E_1 E_2}{E_1 + E_2} \tag{1.46}$$

In which E_1 and E_2 are the spring constants of springs in series and in parallel with dashpot, respectively.

Under the creep test, stress is suddenly applied and maintained at constant value as defined in Eq. (1.17) which yields the following relation considering Eq. (1.43):

$$\sigma = E\varepsilon + \beta E \frac{d\varepsilon}{dt} \tag{1.47}$$

Now Eq. (1.47) can be easily solved and results in:

$$\varepsilon = \frac{\sigma_o}{E} + Ce^{-\frac{t}{\beta}} \tag{1.48}$$

The constant of integration C can be obtained from the initial conditions. Here, one may consider that the sample was not initially strained ($\varepsilon = 0$ at $t = 0$) which results:

$$C = -\frac{\sigma_o}{E} \tag{1.49}$$

Substituting the value of C from Eq. (1.49) in Eq. (1.48) yields:

$$\varepsilon = \frac{\sigma_o}{E}\left(1 - e^{-\frac{t}{\beta}}\right) \tag{1.50}$$

Alternatively, if the strain $\varepsilon = \varepsilon_o$ is suddenly applied on stress free sample ($\sigma = 0$ at t=0) and maintained at a constant value ($\dfrac{d\varepsilon}{dt}=0$ at t=0), then by using Eq. (1.43) one can write:

$$\sigma + \alpha \frac{d\sigma}{dt} = E\varepsilon_o \tag{1.51}$$

and its corresponding solution is

$$\sigma = E\varepsilon_o \left(1 - e^{-\frac{t}{\alpha}} \right) \tag{1.52}$$

On the other hand if we apply harmonic stress $\sigma = \sigma_o e^{i\omega t}$ and strain $\varepsilon = \varepsilon_o e^{i\omega t}$, then solution of equation Eq. (1.43) becomes:

$$\sigma = E\varepsilon_o \left(\frac{1+i\omega\beta}{1+i\omega\alpha} \right) \tag{1.53}$$

which can be simplified to:

$$\sigma = \varepsilon_o \left(E' + i\, E'' \right) \tag{1.54}$$

$$E' = E \left(\frac{1+\omega^2 \beta\alpha}{1+\omega^2 \alpha^2} \right) \tag{1.55}$$

$$E'' = E\omega \left(\frac{\beta-\alpha}{1+\omega^2 \alpha^2} \right) \tag{1.56}$$

As it has been already discussed, there are two unique properties of viscoelastic material; a) Creep and b) Relaxation. Figure (1.10) describes the time history of the creep functions of the above discussed three models and Figure (1.11) describe the time history of the relaxation functions of the above discussed three models. The

24

characteristics of creep function ideally should increase with time and converge to a steady state final value and characteristics of relaxation function ideally should decrease with time and converge to a steady state final value.
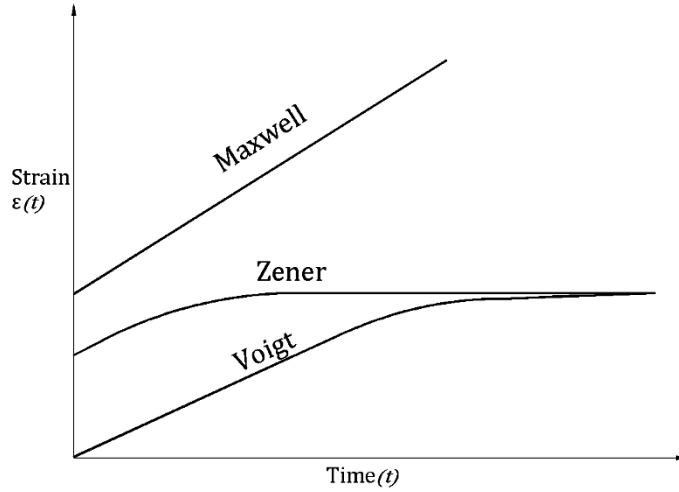
Figure 1.10 Creep function for three models
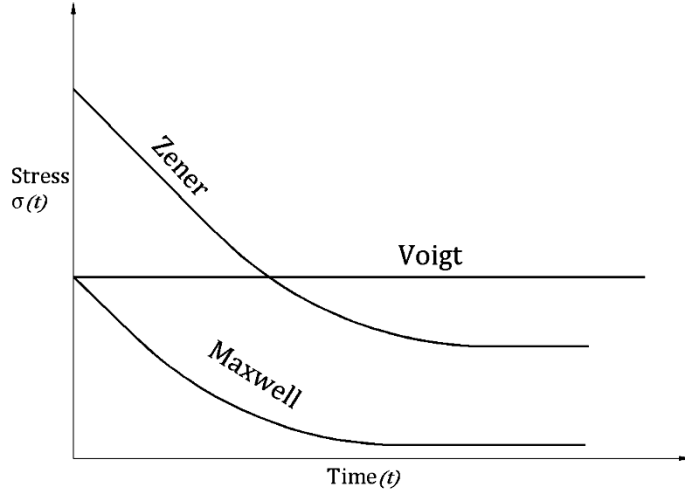
Figure 1.11 Relaxation function for three models

We can easily observe that both, the creep function predicted by the Maxwell model and relaxation function predicted by the Voigt model are impractical. The creep function predicted by the Maxwell model does not converge to steady state value but keep on increasing with time and the relaxation function predicted by the Voigt model keeps constant throughout the time. Therefore, it is clear that both the

Maxwell and Voigt models fail to replicate time domain characteristics of viscoelastic materials, whereas, the Zener model can reasonably predict both creep and relaxation function in time domain.

All three models are able to predict complex modulus in frequency domain; however Zener model better reflects the aspects of real viscoelastic behavior. It should be noted that when we compare the E^* complex modulus to experimental data, the variation with frequency is much more rapid. Therefore, even the Zener model is only an approximation and requires an improvement.

Generalized standard model

The limitation of the simple Zener model can be overcome by considering additional derivate of σ and ε in Eq. (1.43) to give

$$\sigma + \sum_{n=1}^{\infty} \alpha_n \frac{d^n \sigma}{dt^n} = E\varepsilon + E \sum_{n=1}^{\infty} \beta_n \frac{d^n \varepsilon}{dt^n} \qquad (1.57)$$

This generalized standard solid model improves the Zener model but there is major disadvantage as there is substantial number of terms of α_n and β_n that need to be calculated over the wide range of frequencies. This is inconvenient but not impossible.

Fractional Derivates Model

In order to reduce the number of terms needed by the generalized standard model Bagley and Torvik (Bagley, et al., 1983) developed a fractional derivative model to

represent viscoelastic behavior. The complex modulus of viscoelastic material can be represented in Laplace domain as:

$$E^* = \left(\frac{E_o + E_1 s^\alpha}{1 + b s^\beta} \right)$$

(1.58)

The five parameters E_o, E_1, b, α, β are used to accurately curve fit the data acquired through experiments. The advantage of this model is that it accurately fits the experimental data over the wide range of frequency. The model is good in frequency domain only, because it is difficult to take the inverse Laplace transform of a frequency domain complex modulus based on a fractional derivates.

GHM, ATF and ADF Models

The GHM model represents a viscoelastic material by introducing internal variable (Auxiliary dissipation coordinates) to account for viscoelastic relaxation and, thus damping. The shear modulus function in the Laplace domain can be represented as series of mini-oscillatory terms (McTavish, et al., 1993):

$$sG(s) = G_\infty \left(1 + \sum_j^N \hat{\alpha}_j \frac{s^2 + 2\hat{\zeta}_j \hat{\omega}_j s}{s^2 + 2\hat{\zeta}_j \hat{\omega}_j s + \hat{\omega}_j^2} \right)$$

(1.59)

The mini-oscillatory term in summation series depends upon the three material constants $\hat{\alpha}_j$, $\hat{\omega}_j$ and $\hat{\zeta}_j$, which can be evaluated from the curve-fitting of the viscoelastic material master curves. The number of terms N, in the expression is determined from the high or low dependence of the complex modulus.

The ATF modeling method (Lesiutre, et al., 1990) was a time–domain continuum model of material damping that preserves the frequency-dependent damping and modulus of real material. Irreversible thermodynamics processes were used to develop coupled material constitutive equations of evolution. As GHM, ATF also used additional coordinates to predict damping more accurately.

The ADF method was based on a decomposition of the total displacement field into two parts: elastic and anelastic. The anelastic part of displacement describes that part of strain that is not instantaneously proportional to stress. The details of model were presented by Lesieutre and Bianchini (Lesieutre, et al., 1995).

Both ATF and ADF methods lead to first order damping model, which can be implemented only in state space forms when combined with structural analytical models. However, because of second order form, GHM is less efficient as a general model of material behavior. Also, GHM, ATF and ADF methods use additional internal dissipation coordinates which increase degrees of freedom of the system.

1.4.3   Behaviors and Typical Properties of Viscoelastic Material

An understanding of the variation of mechanical and damping properties with frequency and temperature is essential the design of effective vibration control treatments. The following sections will describe how these factors affect the properties of typical viscoelastic material and explain the techniques used to establish the properties of viscoelastic material.

Effect of Temperature

Temperature is considered to be the most important environmental factor affecting the properties of viscoelastic material. This effect can be observed in Figure (1.12) for four distinct regions. The first is the so-called glassy region, where material is dynamically very stiff with high storage modulus but behaves poorly in damping with very low loss factor. The storage modulus in this region changes slowly with temperature, while the loss factor increases rapidly. In the transition region, material changes from glassy state to rubbery state in which the material storage modulus decreases rapidly with temperature, while loss factor attains its maximum value. The third is the rubbery region, here both the modulus and loss factor take somewhat low values and vary insignificantly with temperature. The flow region is typically for a few damping materials, like Vitreous enamels and thermoplastics, here material continues to soften with temperature rise while the loss factor takes on very high value.
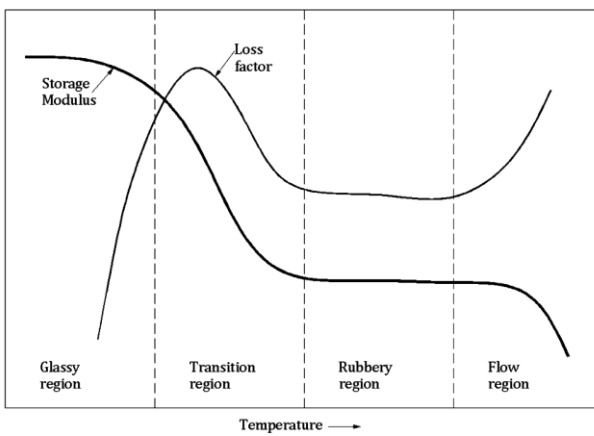
Figure 1.12 Variation of storage modulus and loss factor with temperature (Nashif, et al., 1985)

Effect of Frequency

The most important effect of frequency is that the storage modulus always increases with increasing frequency. It means that viscoelastic materials become dynamically stiffer. The rate of increase is small in both the glassy and rubbery regions, and reaches its maximum in transition region, whereas loss factor first increases with frequency increase, attains its maximum value and then decreases. Variation of the damping properties with frequency at particular temperature is expected to take the form illustrated in Figure (1.13). Examination of Figures (1.13) and (1.14) reveals that, the effect of frequency on storage modulus is qualitatively the inverse of the effect of temperature. To a lesser degree; it takes several decades of frequency to show the same change of behavior as few degree of temperature. This phenomenon is most important aspect of Viscoelasticity. This behavior provides the basis for the temperature-frequency superposition principle that is used to transform material properties from the frequency to temperature domain (Jones, 1990).
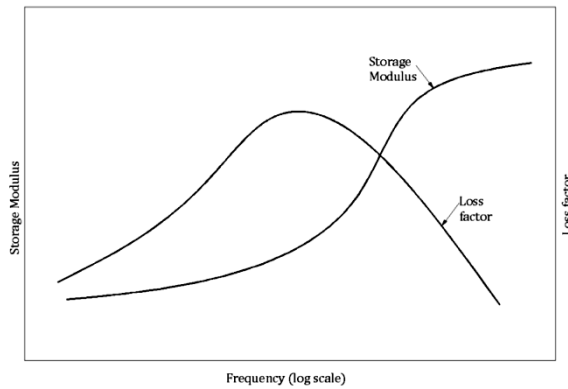
Figure 1.13 Variation of storage modulus and loss factor with frequency (Nashif, et al., 1985)

Combined Effect of Temperature and Frequency

To consider the effect of both frequency and temperature on damping behavior of material, one of the useful techniques for presenting the experimental data is the temperature-frequency equivalence (reduced frequency) principle for linear viscoelastic materials (Ferry, 1980), (Jones, 2001). The principle of temperature-frequency equivalence is based upon assumption that complex modulus values at any given frequency ω_1 and temperature T_1 are similar to those at any other frequency ω_2 and temperature T_2; which must be selected, in such way that:

$$E^*(\omega_1, T_1) = E^*(\omega_2 \alpha(T_2)) \tag{1.60}$$

The factor $\alpha(T)$ is called shift factor of the material and can be determined empirically. The factor $\omega\alpha(T)$ describes the combine effect of both frequency and temperature into a single variable, which is referred as the *reduced frequency.*

One of the most popular shift factor $\alpha(T)$ used to describe the temperature-frequency superposition principle is WLF (Williams-Landel-Ferry) equation which can be written as

$$\log_{10}\left[\alpha(T)\right] = C_1\left(\frac{T - T_{ref}}{C_2 + T - T_{ref}}\right) \tag{1.61}$$

where C_1 and C_2 are constants, and T_{ref} is the reference temperature, to be determined for particular material. The reference temperature T_{ref} can be chosen arbitrarily. Once the parameters of the WLF equation are determined, *master curves* known as nomogram which can display E' (real part of complex modulus) and η

(loss factor) against $\omega\alpha(T)$ (reduced frequency) in one diagram can be created. It is extremely useful and directly used to extrapolate or interpolate the test results between different temperature and frequency.

In the present study, the complex modulus approach is adopted with temperature and frequency dependent values of E' and η. The viscoelastic material used is Viton-B and its properties were obtained from the nomogram as shown in Figure (1.14), (1.15) & Figure (1.16) provided in (Nashif, et al., 1985). Master curves showing real part of complex Young's Modulus E' (Psi) and loss factor η against reduced frequency $f\alpha(T)$ (Hz) and temperature T in Fahrenheit, are digitized. Further values of $\alpha(T)$ shift factor is obtained against temperature T in Fahrenheit by interpolation using neural network toolbox of MATLAB.
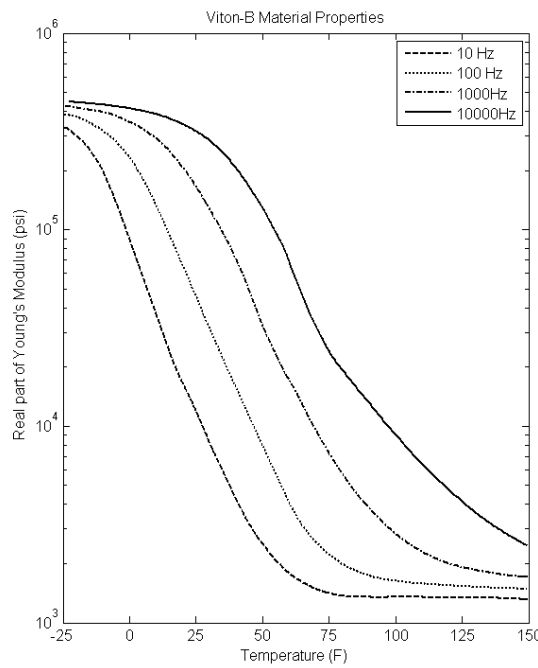
Figure 1.14 Young's Modulus of Viton-B (Nashif, et al., 1985)
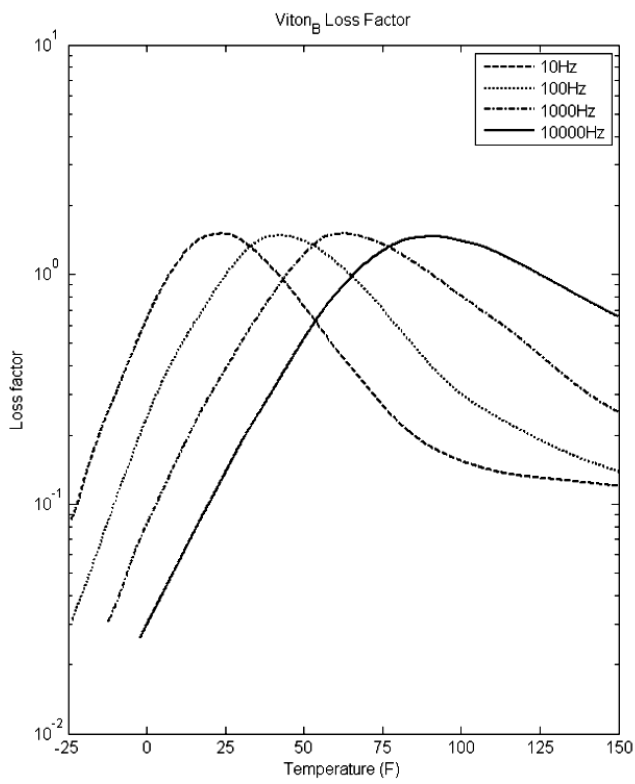
Figure 1.15 Loss factor of Viton-B (Nashif, et al., 1985)
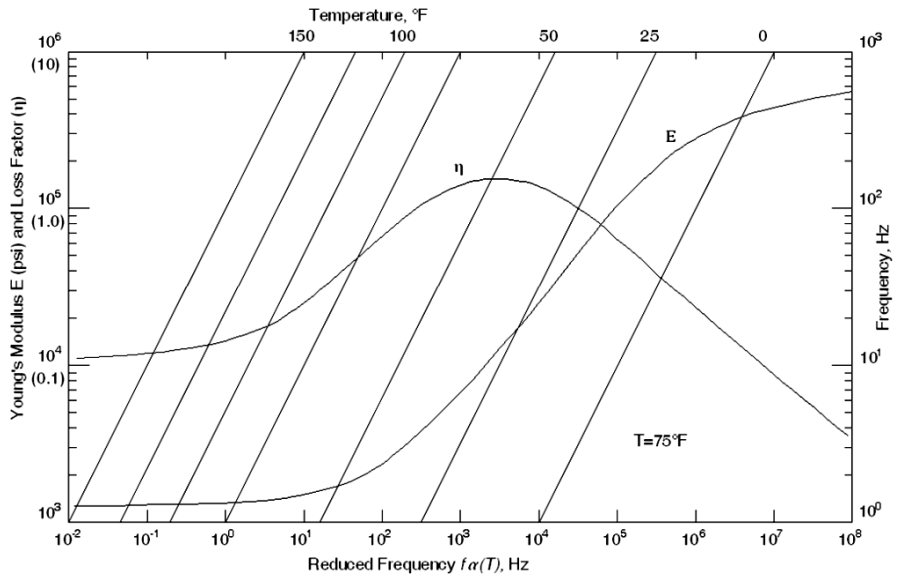
Figure 1.16 Nomogram Viton-B (Nashif, et al., 1985)

1.4.4 Energy Dissipation Mechanism

If sinusoidal force $F(t)$ is applied to a linear viscoelastic structure, then, its result will also be a sinusoidal displacement $X(t)$ with phase difference at the point of force application (Ungar, et al., 1962). Thus we can write:

$$F(t) = F_0 \sin(\omega t + \delta) \tag{1.62}$$

$$X(t) = X_0 \sin(\omega t) \tag{1.63}$$

Now expanding $F(t)$ in Eq. (1.62), one may write:

$$F(t) = X_0 \left(K'(\omega) \sin(\omega t) + K''(\omega) \cos(\omega t) \right) \tag{1.64}$$

where

$$K'(\omega) = \left(\frac{F_0}{X_0} \right) \cos(\delta) \tag{1.65}$$

$$K''(\omega) = \left(\frac{F_0}{X_0} \right) \sin(\delta) \tag{1.66}$$

$K'(\omega)$ is the stiffness derived from the storage modulus of viscoelastic core and $K''(\omega)$ from the loss modulus. Now considering Eq. (1.63) and the identity $\sin^2(\omega t) + \cos^2(\omega t) = 1$, Eq. (1.64) can be written as:

$$\frac{F(t)}{K'(\omega)} = X(t) \pm \frac{K''(\omega)}{K'(\omega)} \left(X_0^2 - X^2(t) \right)^{1/2} \tag{1.67}$$
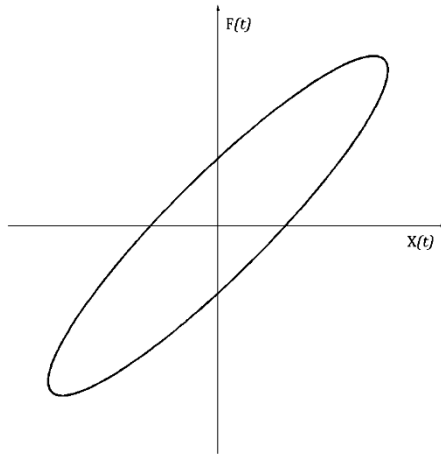
Bishop (Bishop, 1955) has shown that Eq. (1.67) represents an ellipse as shown in Figure (1.18) and the energy D dissipated per cycle is given by:

$$D = \oint FdX = \pi K'' X_0^2 \tag{1.68}$$

Loss Factor

Loss factor of the system can be defined as the ratio of the dissipation energy to the maximum strain energy in the system

$$LF = \frac{\pi K'' X_0^2}{\pi K' X_0^2} = \frac{K''}{K'} \tag{1.69}$$

1.5 Scope of the Present Research

Based on the literature reviews, sandwich beams have been well studied. However improving the effectiveness and accuracy of solutions for these structures is still an active research area. Moreover design optimization of fully and partially treated viscoelastic sandwich beam to efficiently suppress the vibration in a desired frequency range has not received appropriate attention by the research community.

Moreover, few studies have addressed the effect of temperature on vibration characteristics of viscoelastic sandwich beams. Considering above, the main scope of the present research is to systematically address the above mentioned shortages.

As the effectiveness of formulation strongly depends upon the assumptions made, which further depends upon the geometry of structure, the governing equations have been formulated here considering both linear and nonlinear displacement field in the viscoelastic core layer in order to seek some basic guidelines in terms of geometry, boundary conditions and also frequency range where formulations based on linear and nonlinear assumptions deviate from each other. Further, we formulate a formal design optimization methodology to study the effectiveness of partial treated beam, and optimize the parameters like length and location of treated segments for increasing the damping, as partial treatment has great advantage of weigh reduction.

As discussed, the effect of temperature on the viscoelastic material cannot be ignored. In this study, the internal heat generation due the dissipated energy and its effect on vibration and damping characteristics of viscoelastic sandwich beam has been studied. As the viscoelastic sandwich beam deforms, the viscoelastic core layer goes under shear strain which varies along the length of the beam. Areas which go under more strain dissipate more energy and, therefore, heated more. Here, to calculate the temperature gradient developed in the viscoelastic core a finite difference model is developed to gauge the temperature of core along the length of beam.

1.6 Thesis Organization

In the first chapter of this study, literature review and relevant works reported in the literature are highlighted. Also different models representing the mechanical properties of the viscoelastic material are compared. The scope of the dissertation is subsequently formulated on the basis of the reviewed studies. In the second chapter the finite element model for three-node beam element is formulated. Both linear and nonlinear displacement fields are separately considered in the formulations. The validity in finite element formulations is demonstrated by comparing the results with those obtained from experiment available in literatures. Parametric study and comparison between different finite element models are presented according to different thickness of the core layer at different modes. In Chapter 3, partially treated sandwich beam is analyzed using the finite element method and parametric studies are presented to show the damping behavior of the sandwich beam for different configuration of the patches and cuts. The designed optimization problem is then formulated to achieve maximum damping by combining the finite element analysis with genetic algorithm to find the optimum number and the distribution of the patches. In chapter 4, effect of heat dissipation in the core layer is considered by solving the heat equation using finite difference method based on irregular grids. And in the chapter 5, major contribution and conclusion are summarized and finally the recommendations for future studies are discussed.

CHAPTER 2

2 FINITE ELEMENT MODELING OF A SANDWICH BEAM

2.1 Introduction

The analytical solutions are only suitable for very simple structures under homogenous boundary conditions. In reality, it is often desired to design a damped structure with complex geometry, complicated loading and boundary conditions, and also considering material discontinuities within the structures. As a result, it is justified to exploit the benefit of Finite Element Method (FEM) in analyzing the behavior of sandwich structures. In the following section brief literature review regarding the previous study for finite element modeling of sandwich structure is presented. These analyses include definition of displacement field through the thickness of the sandwich structure and implementation of methodology to establish equations of motion using energy principle. Both Hamilton's principle and Lagrange equation can be used to drive equations of motion from energies. Linear and nonlinear modeling has been suggested for displacement field through thickness of viscoelastic layer. These models are explained and also an alternative method is presented to solve differential equations resulting from nonlinear modeling.

2.2 Literature Review

Numerous studies have been done in this area and many finite element techniques have been developed to determine the behavior of sandwich structures. Johnson,

Kienholz and Rogers (Johnson, et al., 1981) have developed the three dimensional brick model for sandwich beams using the MSC/NASTRAN application. They explained the three finite element methods to predict response of damped sandwich structures. The first is the Complex Eigen-value method. In this method, a complex stiffness matrix is formulated by using complex modulus of viscoelastic material, which is not dependent on frequency and is used to determine the free vibration response. An extra damping term can be added to consider viscous damping which varies with frequency. The resulting equations of motion can be then solved as Eigen-value problem with complex Eigen-values and Eigen-vectors.

The next method described was the modal strain energy method. The basic assumption of the modal strain energy method is that the loss factor of damped structure can be predicted by approximating the mode shape of damped structure as that of non-damped structure mode shape. Then, for a particular mode of vibration, the composite loss factor can be obtained by equating the ratio of composite loss factor to the loss factor of viscoelastic material with the ratio of elastic strain energy in the viscoelastic material to the total strain energy in the structure at the time of deformation in a particular non damped mode shape. The modal strain energy method was also adopted by Soni (Soni, 1981) in his finite element analysis. Johnson, Kienholz and Rogers (Johnson, et al., 1981) and Soni (Soni, 1981) presented experimental data to demonstrate their methods on simple problems. But Mace (Mace, 1994) in his study mentioned that this 3D modeling approach can be very complex and costly to implement and highlighted the

difficulties in creating the meshes used for analysis and the complexity of the analysis.

The third finite element method described is that of direct frequency method. In this method harmonically forced vibration response is analyzed using complex stiffness which is frequency dependent. Mace (Mace, 1994) considered very thin viscoelastic layer and neglected the inertial effects of the viscoelastic layer. The stiffness matrix was presented in two separate matrices one for the elastic top and bottom layers and the second a complex stiffness matrix for viscoelastic layer.

In the present study, two finite element models are introduced, which are compatible to both symmetrical and unsymmetrical configuration of sandwich beams. The models are based on discrete displacement approach, which means that all the layers in sandwich structure will have separate displacement field; there is no global displacement field. The compatibility of displacement field is taken care of by maintaining the displacements of all layers at interference boundaries. In the first model, a linear displacement field is assumed, which means all the layers including the viscoelastic core layer have linear displacement variation through the thickness and do not undergo any compression or extension in transverse direction. The second model is based upon the work done by Bai and Sun (Bai, et al., 1995). They incorporated a shear deformation by using a second order displacement field in transverse direction and third order displacement field in axial direction, which allow core to deform in a non-linear way through the thickness. It also allows the core layer to undergo normal compression and extension in transverse direction.

Bai and Sun derived these displacement fields in core from linear elasticity principles by assuming that the axial stress developed in viscoelastic core layer is negligible. They also included the slippage between the layers in their analysis and solved the governing equations analytically. Later Baber, Maddox and Orozco (Baber, et al., 1998) developed the finite element model for sandwich beam using Bai and Sun theory of second order displacement field in core by neglecting the slippage between the layers. They solved the governing differential equation resulted from nonlinear modeling by assuming a very thin viscoelastic core and thus simplifying it to linear equation by ignoring the higher order derivatives. In the present study an alternative method is presented to solve the governing differential equation resulting from nonlinear modeling without ignoring the higher order derivatives. To demonstrate the validity of developed models, validation examples, with various geometries are conducted.

2.3 Finite Element Model Based on Linear Displacement Field at Core Layer (FEM 1)

As, we discussed earlier, the first developed model is based upon the assumption that all the layers of sandwich beam undergo linear displacement variation and there is no compression or extension in the transverse direction.

2.3.1 Kinematics of the model

The geometrical characteristics of a sandwich beam are shown in Figure (2.1). The present model is based upon the following assumptions.

I.   The cross-section of each layer will remain plane after deformation.

II. All layers are perfectly bonded; this means that there is no slippage at the interface of layers.

III. The axial displacement and rotation in top and bottom elastic layers are independent of each other.

IV. The core layer consists of viscoelastic material which is assumed to be incompressible through thickness; this means that the transverse displacement of all layers is same.
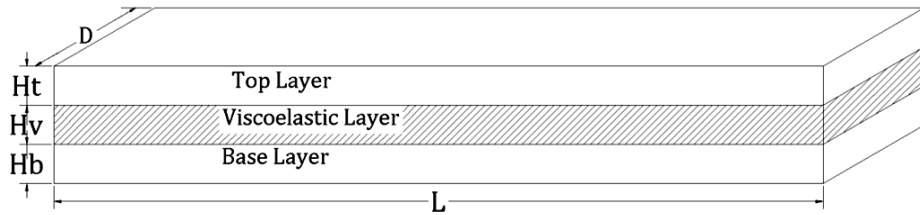
Figure 2.1 Sandwich beam

2.3.2 Displacement fields

Local coordinate system for all three layers is adopted and shown in Figure (2.2). It is noted that the origin of the coordinate system is placed at the centroid of the individual layer. The schematic deformed configurations of the layers are also shown in Figure (2.3).
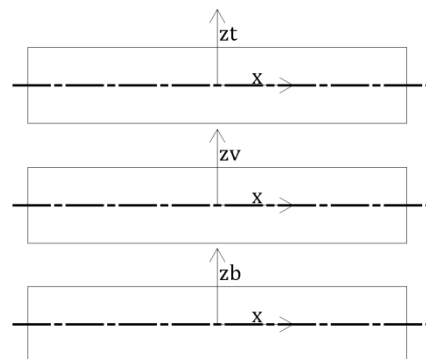
Figure 2.2 Local coordinates in layers

Longitudinal and transverse displacement fields for the base (bottom) layer are given by:

$$u_b(x, z_b, t) = u_b^0(x, t) + z_b \theta_b(x, t) \qquad (2.1)$$

$$w_b(x, z_b, t) = w_b^0(x, t) \qquad (2.2)$$

where

u_b = longitudinal displacement in the base layer for any (x,z) location

u_b^0 = longitudinal displacement at the centroid of the base layer

z_b = distance from centroid of base layer in transverse direction

θ_b = rotation in the base layer

w_b = transverse displacement in the base layer for any (x,z) location

w_b^0 = longitudinal displacement at the centroid of the base layer

Similarly, for the top layer, the displacements are taken as:

$$u_t(x, z_t, t) = u_t^0(x, t) + z_t \theta_t(x, t) \qquad (2.3)$$

$$w_t(x, z_t, t) = w_t^0(x, t) \qquad (2.4)$$

where

43

u_t = longitudinal displacement in the top layer for any (x,z) location

u_t^0 = longitudinal displacement at the centroid of the top layer

z_t = distance from centroid of top layer in transverse direction

θ_t = rotation in the top layer

w_t = transverse displacement in the top layer for any (x,z) location

w_t^0 = longitudinal displacement at the centroid of the top layer

Core layer is made of viscoelastic material and its displacement field may also be described as:

$$u_v(x,z_v,t) = u_v^0(x,t) + z_v\theta_v(x,t) \tag{2.5}$$

$$w_v(x,z_v,t) = w_v^0(x,t) \tag{2.6}$$

where

u_v = longitudinal displacement in the core layer for any (x,z) location

u_v^0 = longitudinal displacement at the centroid of the core layer

z_v = distance from centroid of core layer in transverse direction

θ_v = rotation in the core layer

w_v = transverse displacement in the core layer for any (x,z) location

w_v^0 = longitudinal displacement at the centroid of the core layer

Considering above there would be nine degrees of freedom to describe the displacement field for all layers; however some of the degrees of freedom can easily be eliminated by utilizing the assumption mentioned above. Because of the assumed

perfect bonding of the layers, the axial displacement must remain continuous at the interface between two consecutive layers. To impose this continuity, the subsequent conditions are written:

$$u_v(x, H_v/2, t) = u_t(x, -H_t/2, t) \tag{2.7}$$

$$u_v(x, -H_v/2, t) = u_b(x, H_b/2, t) \tag{2.8}$$

Basically Eq. (2.7) and Eq. (2.8) state the continuity of displacement in axial direction at the interface of viscoelastic layer and top constrained layer and interface of viscoelastic layer and base layer. Using Eq. (2.1), Eq. (2.3) and Eq. (2.5) and considering the continuity conditions in Eqs (2.7) and (2.8) one may write the degrees of freedom associated with the viscoelastic core layer with respect to those of top and bottom layers as:

$$u_v^0(x,t) = 0.5(u_b^0(x,t) + u_t^0(x,t)) + 0.25(H_b\theta_b(x,t) - H_t\theta_t(x,t)) \tag{2.9}$$

$$\theta_v(x,t) = (1/H_v)(u_t^0(x,t) - u_b^0(x,t)) - 0.5(H_t\theta_t(x,t) + H_b\theta_b(x,t)) \tag{2.10}$$

Now, by substituting Eqs (2.9) and (2.10) back into Eq. (2.5), the complete displacement field for viscoelastic core layer in axial direction can be obtained. Here two degree of freedom, one is related to the axial displacement at the neutral axis of viscoelastic core and the other is rotation at the core layer are eliminated in terms of rotation in top and bottom layers and axial displacement at neutral axis of top and bottom layers. Thus applying the displacement continuity at the interfaces can reduce the total number of degrees of freedom from nine to seven. We can further reduce the degrees of freedom by using the assumption that there is no compression in layers in the transverse direction, which means all the layers move the same

displacement in transverse direction. This assumption can reduce the three degrees of freedom in transverse direction to only one degree of freedom as:

$$w_b(x, z_b, t) = w_t(x, z_t, t) = w_v(x, z_v, t) = w^0(x, t) \tag{2.11}$$

Considering above discussion, the generalized degrees of freedom to be used in the analytical formulation can be written as:

$$q = \begin{bmatrix} u_b^0 & \theta_b & u_t^0 & \theta_t & w^0 \end{bmatrix} \tag{2.12}$$

2.3.3   Strain-Displacement relations

Using the assumed expression for displacement fields mentioned before, we can easily formulate the strains developed in all three layers as:

$$\varepsilon_i^{xx} = \frac{\partial u_i}{\partial x} \qquad \varepsilon_i^{yy} = \varepsilon_i^{zz} = 0$$

$$(i = b, v, t) \tag{2.13}$$

$$\gamma_i^{xz} = \frac{\partial u_i}{\partial z} + \frac{\partial w}{\partial x} \quad \gamma_i^{yz} = \gamma_i^{xy} = 0$$

where

ε_i = Axial strain in the ith layer.

γ_i = Shear strain in the ith layer.

Writing Eq. (2.13) for each layer, we have:

$$\varepsilon_b^{xx} = \frac{\partial u_b}{\partial x} \qquad \gamma_b^{xz} = \frac{\partial u_b}{\partial z} + \frac{\partial w}{\partial x} \tag{2.14}$$

$$\varepsilon_t^{xx} = \frac{\partial u_t}{\partial x} \qquad \gamma_t^{xz} = \frac{\partial u_t}{\partial z} + \frac{\partial w}{\partial x} \tag{2.15}$$

$$\varepsilon_v^{xx} = \frac{\partial u_v}{\partial x} \qquad \gamma_v^{xz} = \frac{\partial u_v}{\partial z} + \frac{\partial w}{\partial x} \tag{2.16}$$

in which axial displacement functions for the bottom, top and core layers have been described in Eq.(2.1) , Eq.(2.3) and Eq.(2.5).

2.3.4   Stress –Strain relations

From the strain field obtained previously, the stress field in the beam, according to Hooke's generalized law, is written as:

$$\sigma_i^{xx} = E_i \varepsilon_i^{xx}$$

$$\tau_i^{xz} = G_i \gamma_i^{xz}$$

$$(i = b, v, t) \qquad (2.17)$$

where

E_i = Young's Modulus of the ith layer.

G_i = Shear Modulus of the ith layer.

σ_i = Normal stress in the ith layer.

τ_i = Transversal shear stress in the ith layer.

In case of viscoelastic core layer Young's modulus and shear modulus is complex.

2.3.5   Strain Energy

By taking account of the previously mentioned stress strain behavior, and within the outline of linear elasticity, the internal strain energy of all the three layers can be written as:

$$U_i = \frac{1}{2} \int_V \left(\sigma_i^{xx} \varepsilon_i^{xx} + \tau_i^{xz} \gamma_i^{xz} \right) dV \qquad (2.18)$$

$$(i = b, v, t)$$

$$U_i = \frac{1}{2} D \int_A \left(\sigma_i^{xx} \varepsilon_i^{xx} + \tau_i^{xz} \gamma_i^{xz} \right) dx dz \qquad (2.19)$$

where D is the width of the beam. Now, the total strain energy of the beam can be calculated by the sum of strain energies of each layer in the sandwich beam as:

$$U = U_b + U(\omega)_v + U_t \tag{2.20}$$

As discussed before, the Young's modulus and shear modulus of viscoelastic material depends on excitation frequency ω and so the strain energy of viscoelastic layer $U(\omega)_v$ is also function of ω. Moreover it is important to note that the strain energy $U(\omega)_v$ includes the energy dissipation as well. The stiffness and damping of the system are calculated together by the use of complex shear and Young's modulus for viscoelastic material.

2.3.6 Kinetic Energy

The kinetic energy of all the three layers can be written as:

$$T_i = \frac{1}{2}\rho_i \int_V \left(\dot{u}_i^2 + \dot{w}^2 \right) dV \tag{2.21}$$

$$(i = b, v, t)$$

$$T_i = \frac{1}{2}\rho_i D \int_A \left(\dot{u}_i^2 + \dot{w}^2 \right) dA \tag{2.22}$$

Similarly, the total kinetic energy of the beam can be written as the sum of the kinetic energies of each layer of the sandwich beam as:

$$T = T_b + T_v + T_t \tag{2.23}$$

2.3.7 Work of external forces

Consider uniformly distributed loads P. The associated work is defined by:

$$W = \int_x qPdx \tag{2.24}$$

2.3.8   Finite element formulation based on the linear displacement fields

The finite element formulation of the three layers uniform sandwich beam based on the linear displacement field at the core layer is explained in this section. Beam is discretized into number of elements. The proposed element has three nodes and considering the generalized degrees of freedom $q = \begin{bmatrix} u_b^0 & \theta_b & u_t^0 & \theta_t & w^0 \end{bmatrix}$, each node has five nodal displacement degrees of freedom as shown in Figure (2.4). Three nodes are important as it leads to quadratic interpolation function which eliminates shear locking in the element.

$u1_b^0\ \theta1_b\ u1_t^0\ \theta1_t\ w1^0$ $u2_b^0\ \theta2_b\ u2_t^0\ \theta2_t\ w2^0$ $u3_b^0\ \theta3_b\ u3_t^0\ \theta3_t\ w3^0$
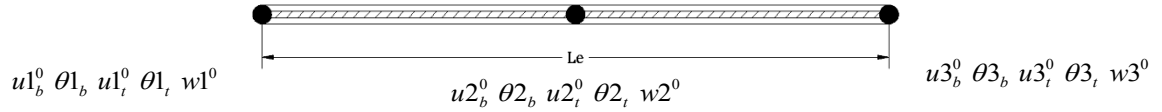
Figure 2.4 Three-node beam element having five degrees of freedom per node

The generalized degrees of freedom q are related to the elementary nodal degrees of freedom q_e through interpolation or shape function matrix N as follows:

$$q = Nq_e \tag{2.25}$$

$$q_e = \begin{bmatrix} u_{1b}^0 & \theta_{1b} & u_{1t}^0 & \theta_{1t} & w_1^0 & u_{2b}^0 & \theta_{2b} & u_{2t}^0 & \theta_{2t} & w_2^0 & u_{3b}^0 & \theta_{3b} & u_{3t}^0 & \theta_{3t} & w_3^0 \end{bmatrix} \tag{2.26}$$

$$N = \begin{bmatrix}
N_1 & 0 & 0 & 0 & 0 & N_2 & 0 & 0 & 0 & 0 & N_3 & 0 & 0 & 0 & 0 \\
0 & N_1 & 0 & 0 & 0 & 0 & N_2 & 0 & 0 & 0 & 0 & N_3 & 0 & 0 & 0 \\
0 & 0 & N_1 & 0 & 0 & 0 & 0 & N_2 & 0 & 0 & 0 & 0 & N_3 & 0 & 0 \\
0 & 0 & 0 & N_1 & 0 & 0 & 0 & 0 & N_2 & 0 & 0 & 0 & 0 & N_3 & 0 \\
0 & 0 & 0 & 0 & N_1 & 0 & 0 & 0 & 0 & N_2 & 0 & 0 & 0 & 0 & N_3
\end{bmatrix} \tag{2.27}$$

where the N_1, N_2 and N_3 are Lagrangian interpolation functions described as:

$$N_1 = -\frac{x}{Le} + 2\left(\frac{x}{Le}\right)^2 \tag{2.28}$$

$$N_2 = 1 - 4\left(\frac{x}{Le}\right)^2 \tag{2.29}$$

$$N_3 = \frac{x}{Le} + 2\left(\frac{x}{Le}\right)^2 \tag{2.30}$$

where, *Le* is the length of the element.

2.3.9 Equations of motion

Here the equations of motion for the element described before have been formulated using the Hamilton's principle:

$$\int_{t_1}^{t_2} \left(\delta(T-U) + \delta W\right)dt = 0 \tag{2.31}$$

By substituting the expression for the kinetic energy, strain energy and work done explained before into Eq. (2.31) and integrating over the time, we obtain:

$$[M_e]\{\ddot{q}_e\} + [K_e(\omega)]\{q_e\} - \{F_e(t)\} = 0 \tag{2.32}$$

where $[M_e]$, $[K_e]$ and $\{F_e\}$ are the element mass matrix, stiffness matrix and force vector, respectively. As discussed above the strain energy of viscoelastic layer is a complex quantity and function of excitation frequency, so the stiffness matrix obtained from the summation of all strain energies is also a function of frequency and is a complex matrix. Thus the stiffness matrix can be split into two matrices as:

$$[M_e]\{\ddot{q}_e\} + [[K'_e(\omega)] + i[K''_e(\omega)]]\{q_e\} - \{F_e(t)\} = 0 \tag{2.33}$$

These element matrices and vectors will be further assembled to obtain the system matrices and vectors to derive equations of motion for the system as:

$$[M]\{\ddot{q}\} + \big([K'(\omega)] + i[K''(\omega)] \big)\{q\} - \{F(t)\} = 0 \tag{2.34}$$

Now let us consider a harmonic load described as:

$$\{F(t)\} = \{F_0\}e^{i\omega t} \tag{2.36}$$

where ω is the frequency of applied harmonic load. Both amplitude and mode of vibration depends on the exciting frequency. It can be assumed that the response due to this applied harmonic load will also be harmonic in nature and at the same frequency. Then:

$$\{q\} = \{Q\}e^{i\omega t} \tag{2.37}$$

$$\{\ddot{q}\} = -\omega^2\{Q\}e^{i\omega t} \tag{2.38}$$

By substituting Eqs. (2.36)-(2.38) into Eq. (2.34), the governing equations of motion can be written as:

$$\big(K'(\omega) + iK''(\omega) - \omega^2 M\big)Q = F_0 \tag{2.39}$$

where the brackets in Eq. (2.39) have been removed for the sake of simplicity with understanding that K' and K'' and M are matrices and Q and F_0 are vector quantities.

Solution of Eq. (2.39) can easily be obtained for every frequency after applying the corresponding boundary conditions by using the inverse of the matrix inside the parenthesis on the left hand side. But generally, we are not interested in the response for every exciting frequency. Only when the exciting frequency gets closer to the natural frequency of the system, the response of the system elevated as inertial forces become prominent along external exciting forces. Natural frequencies and the associated mode shapes of the system can be obtained by equating the exciting force amplitude in the Eq. (2.36) to zero as:

$$\left(K'(\omega) + iK''(\omega) - \omega^2 M\right)Q = 0 \qquad\qquad (2.40)$$

This equation cannot be solved directly as eigen value problem to obtain natural frequencies because the stiffness matrix is implicitly dependent on the frequency itself, which makes the problem nonlinear and iteration method should be adopted. A very efficient inverse iteration method was described by Chen and Chan (Chen, et al., 2000) to calculate the eigen values (natural frequencies) and corresponding eigenvectors. This method has been utilized in this study and has been briefly explained here. With a starting value of ω_0 , the iteration procedure is as follows:

1. $n \to 0 \qquad , \quad \omega_n \to \omega_0$

2. Calculate $K_n = K'(\omega) + iK''(\omega)$

3. Inverse iteration for the generalized linear eigenvalue problem

   $$[K_n - \omega_n^2 M]\psi_{n+1} = [\omega_{n+1}^2 - \omega_n^2]M\psi_{n+1}$$

   where ψ_{n+1} is a complex eigenvector. The complex eigenvalue is then updated by

   $$\omega_{n+1}^2 = \frac{\psi'_{n+1}K_n\psi_{n+1}}{\psi'_{n+1}M\psi_{n+1}}$$

4. Continue steps 1 through 3 until the following convergence is approached

   $$\frac{\left|\omega_{n+1}^2 - \omega_n^2\right|}{\omega_n^2} \le \Delta \quad , \quad \Delta = 10^{-5}$$

Once the eigenvalues and the corresponding eigenvectors are obtained, one could easily determine the natural frequencies and the corresponding modal loss factors and the vibration response.

2.4 Finite Element Model Based on Nonlinear Displacement Field at Core Layer (FEM 2)

The viscoelastic Young's modulus is very low as compared to elastic layers, so by ignoring the axial longitudinal stress in viscoelastic layer and by following the elasticity analysis, Bai and Sun (Bai, et al., 1995) has developed a nonlinear variation of displacement field for viscoelastic core layer. The model allows the viscoelastic layer to undergo compression in transverse direction and permits a more general shear deformation through thickness of the core to accommodate thicker core layer. They also considered an imperfect adhesive layer between the interference of the core and top & base layers. Because the adhesive layer thickness is very low comparing to the viscoelastic core layer, the effect of adhesive layer is not significant unless the adhesive layer is significantly softer than the core layer. For this reason perfect bonding between the layers at interference is suitable assumption for most sandwich beams.

2.4.1 Displacement field

Local coordinate system for all three layers is adopted and shown in Figure (2.2). Origin of the coordinate system is placed at the centroid of the individual layer. The longitudinal and transverse displacement fields for the base and top constrained layers are the same as those given in Eqs. (2.1)-(2.4).

Core layer is made of viscoelastic material and its displacement field is derived by linear elasticity analysis by assuming that the axial stress in the viscoelastic core layer is negligible (Bai, et al., 1995):

$$u_v(x,z_v,t)=u_v^0(x,t)+z_v\left(e\alpha(x,t)-\frac{\partial w_v^0(x,t)}{\partial x}\right)-\frac{z_v^2}{2}\frac{\partial\beta(x,t)}{\partial x}+\frac{z_v^3}{6}\frac{\partial^2\alpha(x,t)}{\partial x^2} \qquad (2.41)$$

$$w_v(x,z_v,t)=w_v^0(x,t)+z_v\beta(x,t)-\frac{z_v^2}{2}\frac{\partial\alpha(x,t)}{\partial x} \qquad (2.42)$$

where

$u_v=$ longitudinal displacement in the core layer for any (x,z) location

$u_v^0=$ longitudinal displacement at the centroid of the core layer

$z_v=$ distance from centroid of core layer in transverse direction

$\alpha=$ shear deformation in core

$\beta=$ transverse normal deformation in core

$w_v=$ transverse displacement in the core layer for any (x,z) location

$w_v^0=$ transverse displacement at the centroid of the core layer

$e=2(1+\upsilon_v)$

$\upsilon_v=$ Poisson ratio of viscoelastic core.

As it can be realized to describe the displacement field for the core layer, four generalized degrees of freedom u_v^0, w_v^0, α and β are required. Unlike linear model where transverse displacement of all layers are the same and continuity of only axial displacement at interference of layers was considered, here, nonlinear displacement field of core viscoelastic layer allows the transverse displacement of top constrained layer and base layer to remain independent of each other. That led to transversal compression and extension of core layer. But still the continuity of axial and transverse displacement prevails at the interface of layers which lead to

boundary condition equations for axial displacement as discussed earlier in Eq. (2.7) and Eq. (2.8) and for transverse displacement as follows:

$$w_v(x, H_v/2, t) = w_t^0(x, -H_t/2, t) \tag{2.43}$$

$$w_v(x, -H_v/2, t) = w_b^0(x, H_b/2, t) \tag{2.44}$$

After substituting the displacement fields of the core layer from Eq. (2.41) and Eq. (2.42) into Eqs (2.7), (2.8), (2.43), and (2.44), it is possible to eliminate three of the four degrees of freedom in the core explicitly through the following relations

$$u_v^0 = \frac{1}{2}\left(u_t^0 + u_b^0 - \left(\frac{H_t}{2} + \frac{H_v}{4} \right)\theta_t + \left(\frac{H_b}{2} + \frac{H_v}{4} \right)\theta_b \right) \tag{2.45}$$

$$w_v^0 = \frac{w_t^0 + w_b^0}{2} + \frac{H_v^2}{8}\frac{\partial \alpha}{\partial x} \tag{2.46}$$

$$\beta = \frac{w_t^0 - w_b^0}{H_v} \tag{2.47}$$

The fourth degree of freedom for the core layer, $\alpha(x,t)$, cannot be eliminated directly; but it is related to the variables of top and base layers by the following partial differential equation:

$$\frac{\partial^2 \alpha(x,t)}{\partial x^2} - \frac{12}{H_v^2}\alpha = \frac{12}{H_v^3}\left(u_b^0 - u_t^0 + \frac{(H_t + H_v)}{2}\theta_t + \frac{(H_b + H_v)}{2}\theta_b \right) \tag{2.49}$$

Considering above discussion, the generalized degrees of freedom, q for the case of nonlinear model can be described as:

$$q = \begin{bmatrix} u_b^0 & \theta_b & w_b^0 & u_t^0 & \theta_t & w_t^0 \end{bmatrix} \tag{2.50}$$

It should be noted that the partial differential equation in Eq. (2.49) can be converted into the ordinary differential equation for steady state harmonic response (independent of variable time t) as:

$$\frac{d^2\alpha(x)}{dx^2} - \frac{12}{H_v^2}\alpha = \frac{12}{H_v^3}\left(u_b^0 - u_t^0 + \frac{(H_t + H_v)}{2}\theta_t + \frac{(H_b + H_v)}{2}\theta_b\right) \tag{2.51}$$

Solution of the obtained ordinary differential equation is given by the sum of homogeneous solution α_h and particular solution α_p which is discussed in the next section.

2.4.2 Finite element formulation

Here the finite element formulation of the three layers uniform sandwich beam based on the nonlinear displacement distribution at the viscoelastic core layer is discussed. Beam is discretized into number of elements. Similar to the linear formulation, the proposed element has three nodes and considering the generalized degrees of freedom given in Eq. (2.50), each node has six nodal displacement degrees of freedom as shown in Figure (2.5).
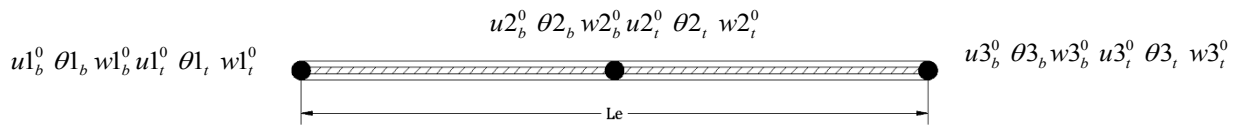
Figure 2.5 Three-node beam element having six degrees of freedom per node

The generalized degrees of freedom q are related to the elementary degrees of freedom q_e through the shape function matrix N as follows

$$q = Nq_e \tag{2.52}$$

$$q_e = \begin{bmatrix} u1_b^0 & \theta1_b & w1_b^0 u1_t^0 & \theta1_t & w1_t^0 u2_b^0 & \theta2_b & w2_b^0 u2_t^0 & \theta2_t & w2_t^0 u3_b^0 & \theta3_b & w3_b^0 u3_t^0 & \theta3_t & w3_b^0 \end{bmatrix} \tag{2.53}$$

$$N = \begin{bmatrix} N1 & 0 & 0 & 0 & 0 & 0 & N2 & 0 & 0 & 0 & 0 & 0 & N3 & 0 & 0 & 0 & 0 & 0 \\ 0 & N1 & 0 & 0 & 0 & 0 & 0 & N2 & 0 & 0 & 0 & 0 & 0 & N3 & 0 & 0 & 0 & 0 \\ 0 & 0 & N1 & 0 & 0 & 0 & 0 & 0 & N2 & 0 & 0 & 0 & 0 & 0 & N3 & 0 & 0 & 0 \\ 0 & 0 & 0 & N1 & 0 & 0 & 0 & 0 & 0 & N2 & 0 & 0 & 0 & 0 & 0 & N3 & 0 & 0 \\ 0 & 0 & 0 & 0 & N1 & 0 & 0 & 0 & 0 & 0 & N2 & 0 & 0 & 0 & 0 & 0 & N3 & 0 \\ 0 & 0 & 0 & 0 & 0 & N1 & 0 & 0 & 0 & 0 & 0 & N2 & 0 & 0 & 0 & 0 & 0 & N3 \end{bmatrix} \quad (2.54)$$

Until now the shear deformation α has not been explicitly written in terms of q. To do this, first let us discuss about the homogenous and particular solutions for α according to Eq. (2.51). The homogenous solution of Eq. (2.51) can easily be calculated as

$$\alpha_h = A_1 e^{\sqrt{\frac{12e}{H_v^2}}x} + A_2 e^{-\sqrt{\frac{12e}{H_v^2}}x} \quad (2.55)$$

As, we can see none of degrees of freedom are included in the exponential terms, which suggests that the homogenous solution of the Eq. (2.51) has less influence and can be ignored. Moreover it was discussed by Baber, Maddox, and Orozco (Baber, et al., 1998) that α_h dissipate rapidly from the boundaries. The particular solution can be approximated by the polynomial series and here is regarded as the total solution:

$$\alpha \approx \alpha_p = a_0 + a_1 x + a_2 x^2 \quad (2.56)$$

The coefficient of Eq. (2.56) can easily be derived by replacing α_p as a polynomial series and the generalized degrees of freedom in terms of elementary degrees of freedom q_e in Eq. (2.51) and then equating the coefficient of x^0, x^1 and x^2 from both sides of equation. The detail of the coefficient is provided in the Appendix A.

2.4.3 Strain-Displacement relations

Using the assumed expression for displacement fields mentioned above, we can easily formulate the strains developed in all three layers. It should be noted that, because of nonlinear displacement field in core, normal strain in the transverse direction in core layer is not zero anymore:

$$\varepsilon_i^{xx} = \frac{\partial u_i}{\partial x} \qquad \varepsilon_i^{yy} = 0 \quad \varepsilon_v^{zz} = \frac{\partial w_v}{\partial x}$$

$$(i = b, v, t) \qquad (2.57)$$

$$\gamma_i^{xz} = \frac{\partial u_i}{\partial z} + \frac{\partial w_i}{\partial x} \quad \gamma_i^{yz} = \gamma_i^{xy} = 0$$

where

ε_i = Axial strain in the ith layer.

γ_i = Shear strain in the ith layer.

Eq. (2.57) can be extended for the bottom, top and core layers as:

$$\varepsilon_b^{xx} = \frac{\partial u_b}{\partial x} \qquad\qquad\qquad \gamma_b^{xz} = \frac{\partial u_b}{\partial z} + \frac{\partial w}{\partial x} \qquad\qquad (2.58)$$

$$\varepsilon_t^{xx} = \frac{\partial u_t}{\partial x} \qquad\qquad\qquad \gamma_t^{xz} = \frac{\partial u_t}{\partial z} + \frac{\partial w}{\partial x} \qquad\qquad (2.59)$$

$$\varepsilon_v^{xx} = \frac{\partial u_v}{\partial x} \quad \varepsilon_v^{zz} = \frac{\partial w_v}{\partial z} \qquad \gamma_v^{xz} = \frac{\partial u_v}{\partial z} + \frac{\partial w}{\partial x} \qquad (2.60)$$

in which axial displacement functions have been described in Eqs. (2.1)-(2.4) for the top and bottom layers and Eqs (2.41) and (2.42) for the viscoelastic core layer.

2.4.4 Strain Energy

By taking account the previously mentioned stress strain behavior in Eqs. (2.58)-(2.60), and within the outline of linear elasticity, the internal strain energy of the top and bottom layers can be written as:

$$U_i = \frac{1}{2} \int_V \left(\sigma_i^{xx} \varepsilon_i^{xx} + \tau_i^{xz} \gamma_i^{xz} \right) dV \qquad (2.61)$$

$$(i = b, t)$$

$$U_i = \frac{1}{2} D \int_A \left(\sigma_i^{xx} \varepsilon_i^{xx} + \tau_i^{xz} \gamma_i^{xz} \right) dx dz \qquad (2.62)$$

The strain energy in the core layer has additional term related to the normal strain developed in transverse direction and is given by

$$U_v = \frac{1}{2} \int_V \left(\sigma_v^{zz} \varepsilon_v^{zz} + \tau_v^{xz} \gamma_v^{xz} \right) dV \qquad (2.63)$$

$$U_v = \frac{1}{2} D \int_A \left(\sigma_v^{zz} \varepsilon_v^{zz} + \tau_v^{xz} \gamma_v^{xz} \right) dx dz \qquad (2.64)$$

where again D is the width of the beam. As mentioned before in section 2.4, the axial longitudinal stress in viscoelastic layer has been ignored for this case.

The total strain energy of the beam can be calculated by the sum of strain energies of each layer in the sandwich beam as:

$$U = U_b + U(\omega)_v + U_t \qquad (2.65)$$

2.4.5 Equation of motion

There is no change in the formulation of kinetic energy as compared with that for linear model so; the kinetic energy of all the three layers is formulated as mentioned in Eq. (2.23).

Equation of motion for element can be formulated using the Hamilton's principle given in Eq. (2.31). The detail of matrices developed is provided in appendix A. As discussed in section (2.3.9), the equations can be solved by the same technique for harmonic loading and free vibration. Only difference arises for the transverse response because the top and base layer undergoes different displacement, and

hence, average response of both layers is considered to calculate the transverse displacement.

2.5   Modal Loss factor

Loss factor for the each mode can be obtained by definition defined in (Ungar, et al., 1962) as the ratio of dissipation energy to the maximum strain energy in a cycle for particular mode and can be extended to finite element model using Eq. (1.69) discussed in Chapter 1:

$$LF_m = \frac{\psi'_m K''_m \psi_m}{\psi'_m K'_m \psi_m} \qquad\qquad m= 1,2,3,...$$

where *m* is the mode number.

2.6   Numerical Results and Validation

This section presents validation cases for the presented finite element models for the viscoelastic sandwich beam. Fifteen elements are used to represent the sandwich beam. The Finite element model based on the linear and non-linear displacement fields at core are referred as FEM 1 and FEM 2, respectively.

The natural frequencies and loss factor of fully treated sandwich beam with clamped free boundary conditions is compared to the experimental data (referred to as Exp) provided by Leibowitz and Lifshitz (Leibowitz, et al., 1990) and results of numerical model (referred to as Num) developed by Lifshitz and Leibowitz (Lifshitz, et al., 1987). Leibowitz and Lifshitz provided experimental data and numerical results from their finite element model based on linear displacement fields at core layer for cantilever sandwich beam with various configurations. The length and width of

beams in all configurations remain constant and are 180 mm and 12mm, respectively. The heights of all three layers for various beams are provided in Table 2.1.

Table 2.1 Geometric Configuration of beams (Leibowitz, et al., 1990)

Beam	H_b (mm)	H_v (mm)	H_t (mm)
1A	4.5	0.7	1.1
2A	5.5	0.8	2.0
4A	3.7	1.2	3.7
7A	1.0	2.7	5.0
10A	2.0	3.0	5.0
11A	4.0	1.7	4.0

The sandwich beams are made by molding a Neoprene CR-602 layer between the 2024 Aluminum layers. The Young's modulus E= 71 GPa and density 2766 Kg/m^3 is used for Aluminum layers. The density of Neoprene is taken as 1230 Kg/m^3 and dynamic properties of the viscoelastic core provided in (Leibowitz, et al., 1990) are given by

$G'(f) = 1.007 \times 10^{-3} f + 1.386$ MPa (2.67)

$\eta(f) = 1.608 \times 10^{-4} + 0.256$ (2.68)

The natural frequency and loss factor for each mode is calculated by method described in section 2.3.9. Figures (2.6) and (2.7) show the first and second natural frequencies using FEM1 and FEM2 for different configurations and their compassion with numerical and experimental results reported in the literature.
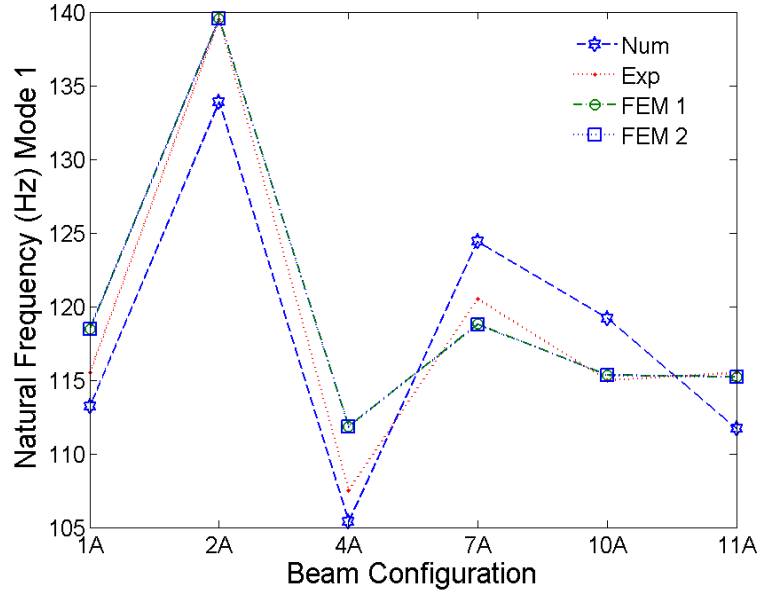
Figure 2.6 Comparison of first Natural frequency of clamped free with experimental data (Leibowitz, et al., 1990) and numerical results (Lifshitz, et al., 1987)
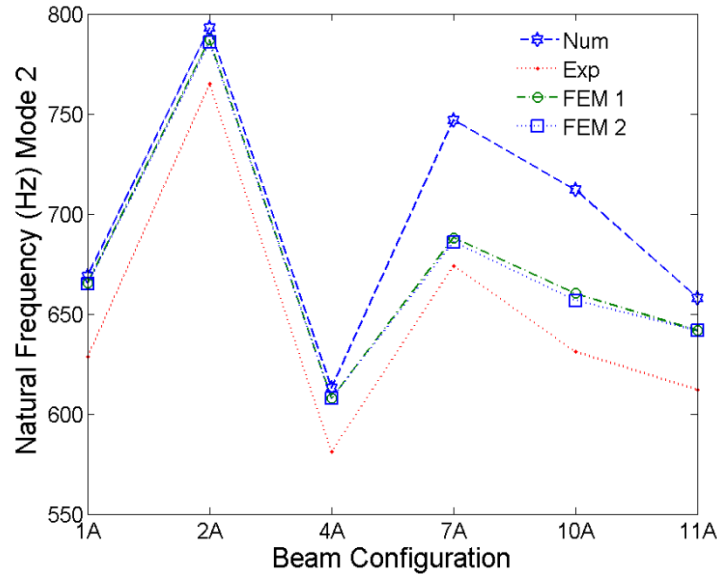
Figure 2.7 Comparison of second Natural frequency of clamped free with experimental data (Leibowitz, et al., 1990) and numerical results (Lifshitz, et al., 1987)

The presented results clearly demonstrate that the frequencies calculated by the presented FEM models are in accordance with experimental results for various beam configurations. In fact, the second natural frequency based on the FEM 2 is closer to the experimental data than that based on FEM 1, as the thickness of the

core layer increases in the configuration 7A and 10A. This shows that FEM2 model provides more accurate results for thick viscoelastic core.

The loss factor for all beam configurations is also compared with experimental data and numerical results. Figures (2.8) and (2.9) also shows the loss factors for modes 1 and 2 for different sandwich beam configurations and their comparison with experimental and numerical results reported in the literature.
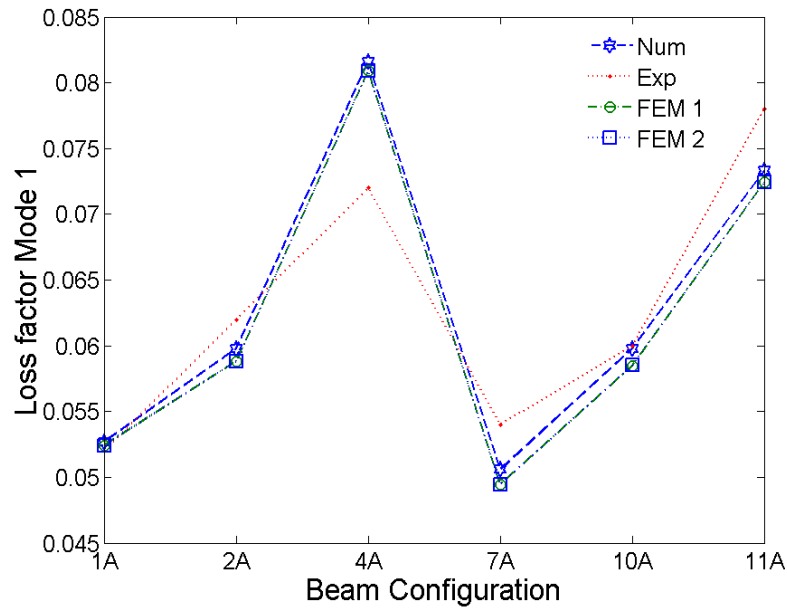
Figure 2.8 Comparison of Loss factor (Mode1) of clamped free with experimental data (Leibowitz, et al., 1990) and numerical results (Lifshitz, et al., 1987)
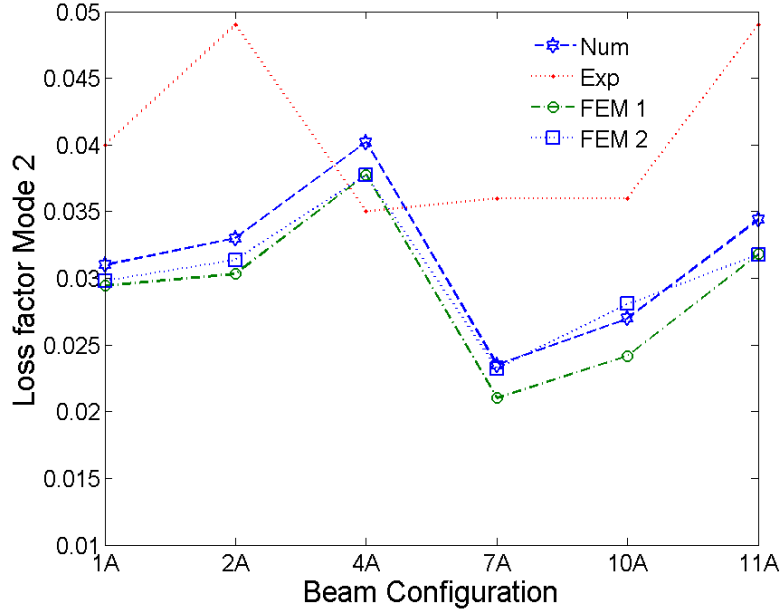
Figure 2.9 Comparison of Loss factor (Mode1) of clamped free with experimental data (Leibowitz, et al., 1990) and numerical results (Lifshitz, et al., 1987)

As it can be realized, the agreement between simulated and experimental loss factors is not good, particularly in the case of second mode. This can be attributed to the fact that damping measurement are known to have large variation, which become larger for higher modes. Moreover the internal structural damping in the elastic layers of aluminum is not considered in FEM models, which can lead to some differences with the experimental readings.

2.7   Parametric studies and Comparison of FEM 1 and FEM 2 models

Having established confidence in the FEM models for calculating the modal parameters like natural frequency and loss factor, we can now investigate for the effect of varying the height of viscoelastic core layer under various boundary conditions. As we have already observed in Figs. (2.7) and (2.9) for beam 7A and 10A which have thicker core layer, non-linear displacement field in the core provides more accurate results for natural frequency and loss factor at mode 2. This

64

difference between the two FEM models and more accuracy of nonlinear displacement field at relatively thick core encourages us to further investigate the accuracy of FEM model with linear displacement field compared with the nonlinear displacement field at the core for higher modes under different boundary conditions. Thickness of the core has practical importance, as the damping of the structure is mainly due to the viscoelastic layer. We will investigate the results for natural frequencies and loss factors of sandwich beam with varying height of viscoelastic core layer for the first three modes considering two boundary conditions (Clamped-Free and Clamped-Clamped) using both linear and nonlinear FEM models. The base and top constrained layers are made of Aluminum and viscoelastic core layer is made of Neoprene CR-602 which is similar to the material chosen by Leibowitz and J.M. in their experiment (Leibowitz, et al., 1990). The mechanical properties of the materials are similar to those given in section 2.6. The geometric dimension of layers for the sandwich beam is provided in Table 2.2

Table 2.2 Geometric dimension in (mm) of sandwich beams for analysis

Geometric Dimension of Sandwich Beams for comparison analysis		
Specification	Clamped-Free Beam	Clamped-Clamped Beam
(Length of Beam) L	180	360
(Width of Beam) D	15	15
(Height of base layer) H_b	5	5
(Height of top constrained layer) H_t	2.5	2.5
(Ratio of core layer to base layer heights) H_v/H_b	Varies (0.1 to 2)	Varies (0.1 to 2)

A comparison of the natural frequencies and Loss factors of the sandwich beams with different thickness of viscoelastic layer for the clamped- free and clamped-clamped end conditions for the first three modes has been performed and results

are shown in Figures (2.10) to (2.15) for the clamped-free sandwich beam and in Figures (2.16) to (2.21) for the clamped- clamped sandwich beam.
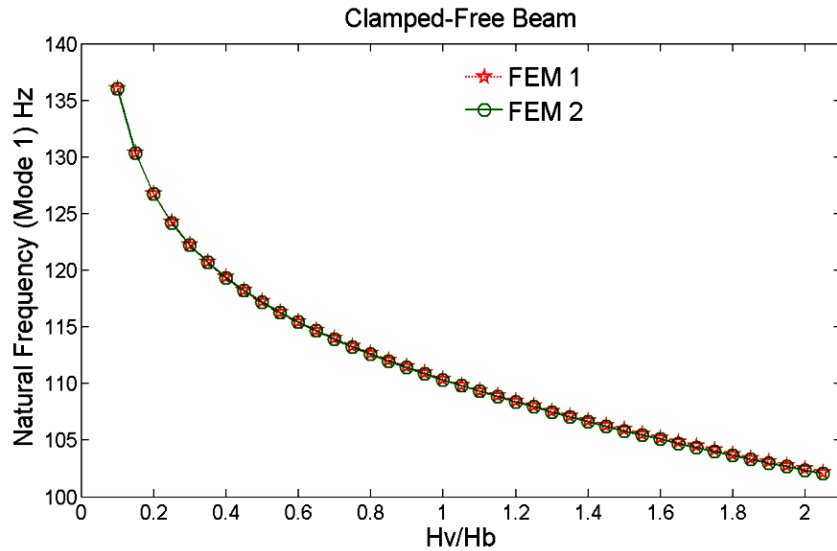
Figure 2.10 Comparison of first Natural Frequencies obtained by FEM1 and FEM2 models, by varying ratio of viscoelastic core to base layer heights for Clamped-Free beam
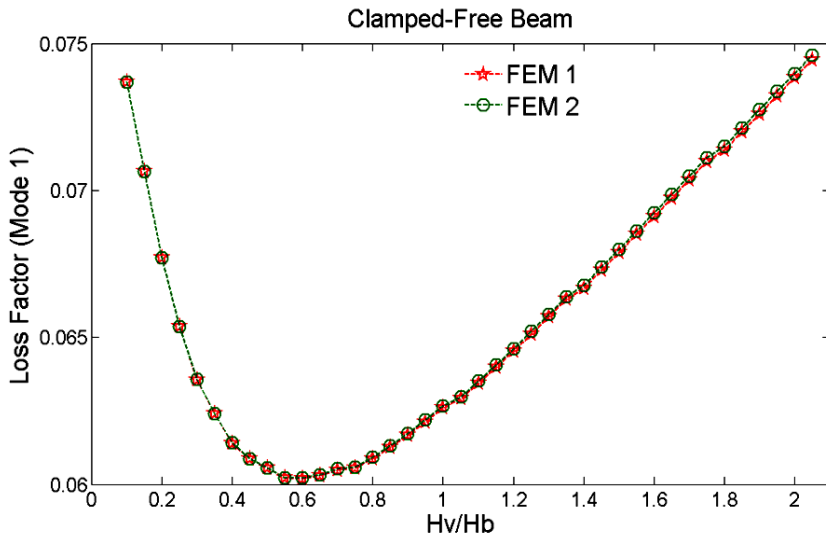
Figure 2.11 Comparison of Loss Factors (mode 1) obtained by FEM1 and FEM2 models, by varying ratio of viscoelastic core to base layer heights for Clamped-Free beam
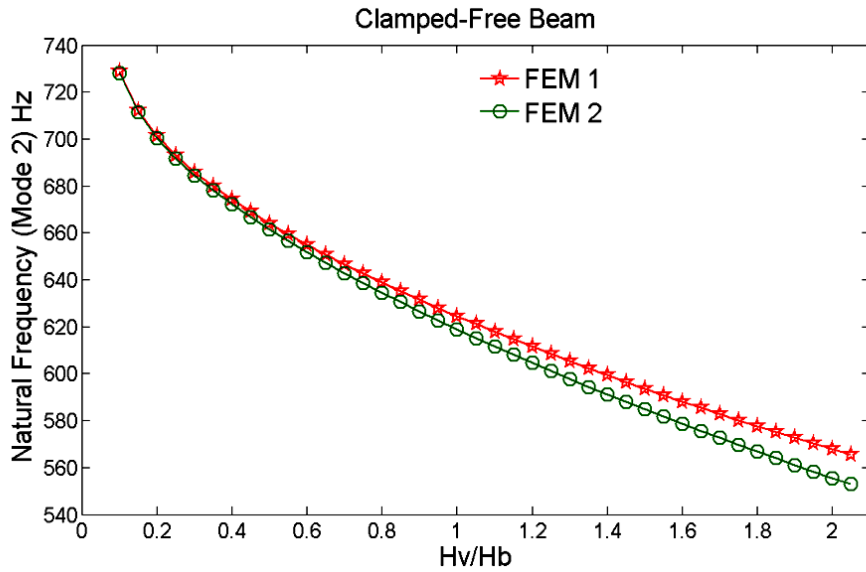
Figure 2.12 Comparison of second Natural Frequencies obtained by FEM1 and FEM2 models, by varying ratio of viscoelastic core to base layer heights for Clamped-Free beam
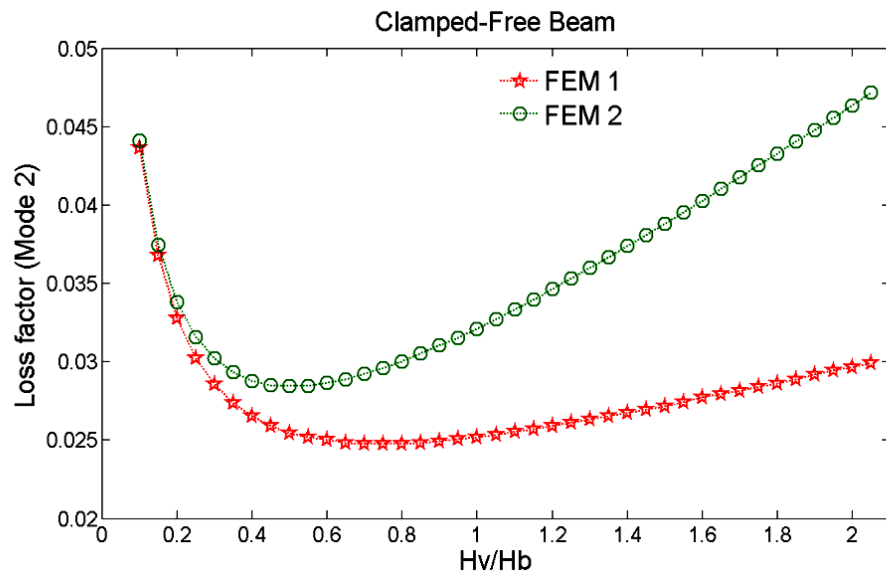
Figure 2.13 Comparison of Loss Factors (mode 2) obtained by FEM1 and FEM2 models, by varying ratio of viscoelastic core to base layer heights for Clamped-Free beam
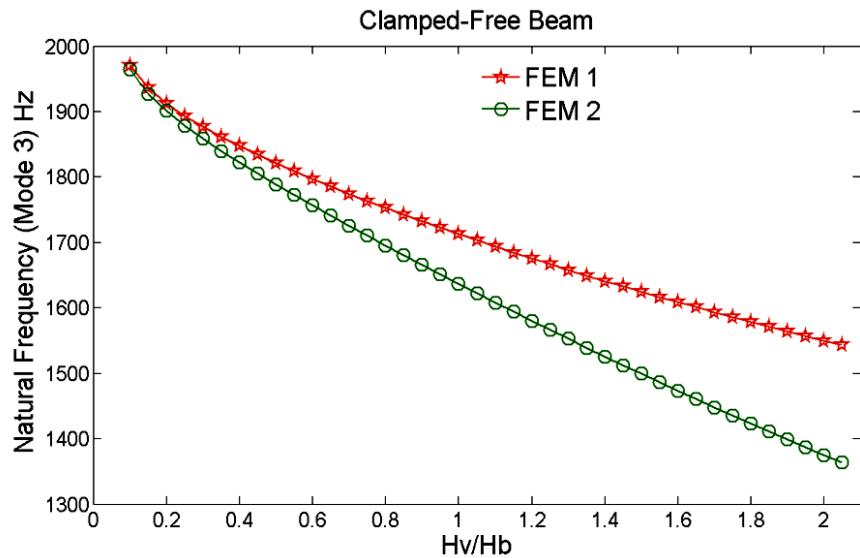
Figure 2.14 Comparison of third Natural Frequencies obtained by FEM1 and FEM2 models, by varying ratio of viscoelastic core to base layer heights for Clamped-Free beam
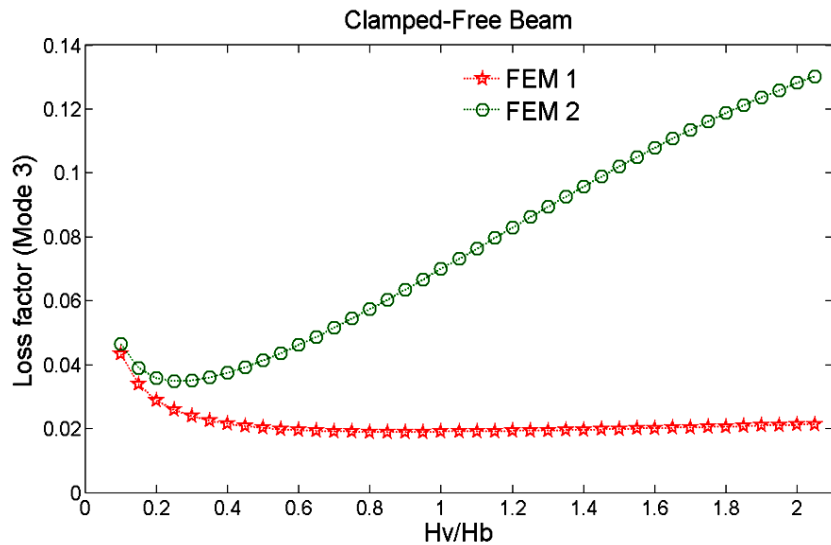
Figure 2.15 Comparison of Loss Factors (mode 3) obtained by FEM1 and FEM2 models, by varying ratio of viscoelastic core to base layer heights for Clamped-Free beam

68
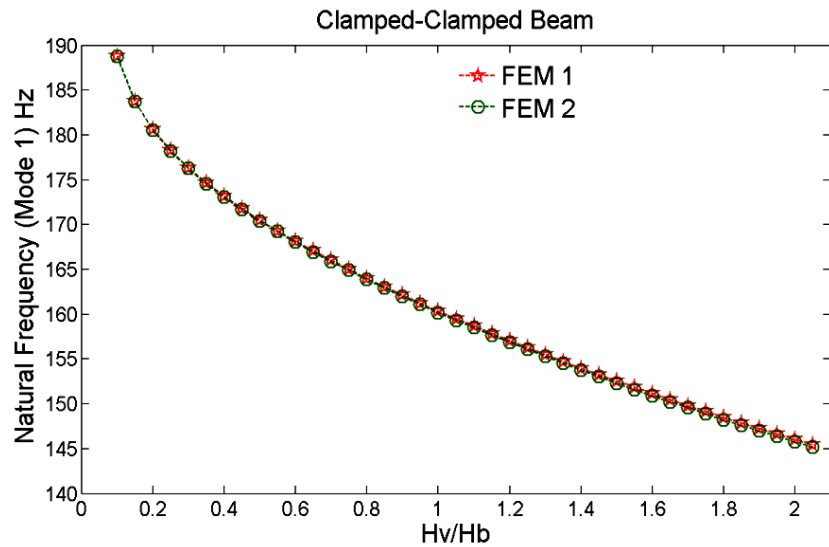
Figure 2.16 Comparison of first Natural Frequencies obtained by FEM1 and FEM2 models, by varying ratio of viscoelastic core to base layer heights for Clamped-Clamped beam
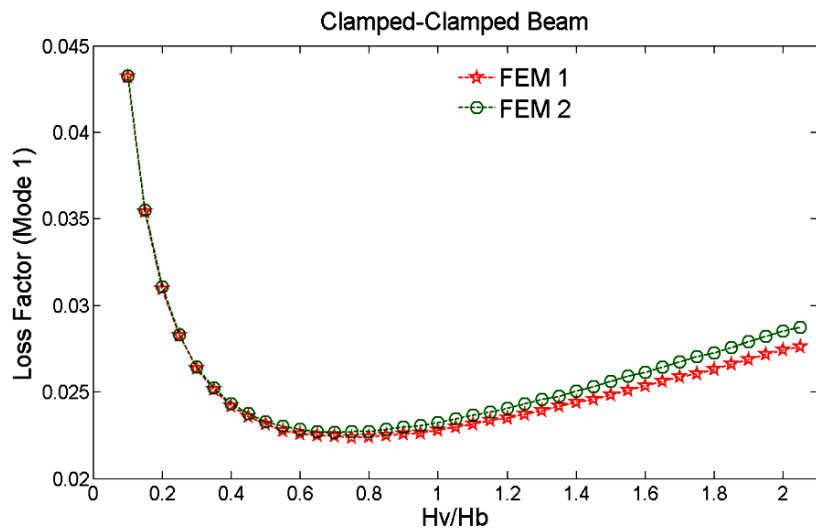
Figure 2.17 Comparison of Loss Factors (mode 1) obtained by FEM1 and FEM2 models, by varying ratio of viscoelastic core to base layer heights for Clamped-Clamped beam
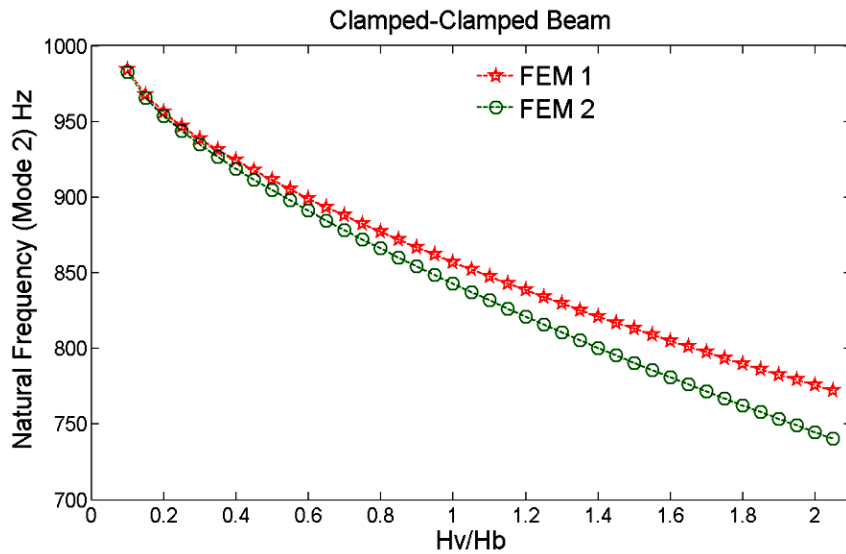
Figure 2.18 Comparison of second Natural Frequencies obtained by FEM1 and FEM2 models, by varying ratio of viscoelastic core to base layer heights for Clamped- Clamped beam
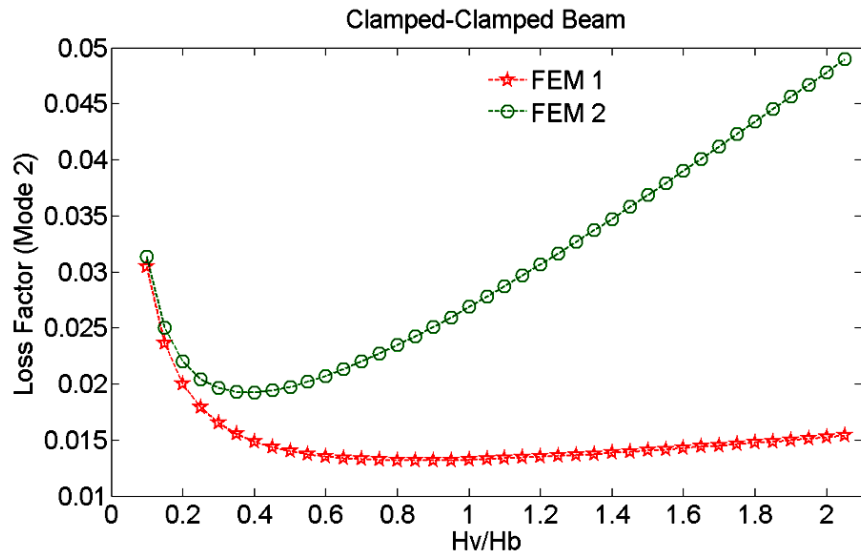
Figure 2.19 Comparison of Loss Factors (mode 2) obtained by FEM1 and FEM2 models, by varying ratio of viscoelastic core to base layer heights for Clamped- Clamped beam
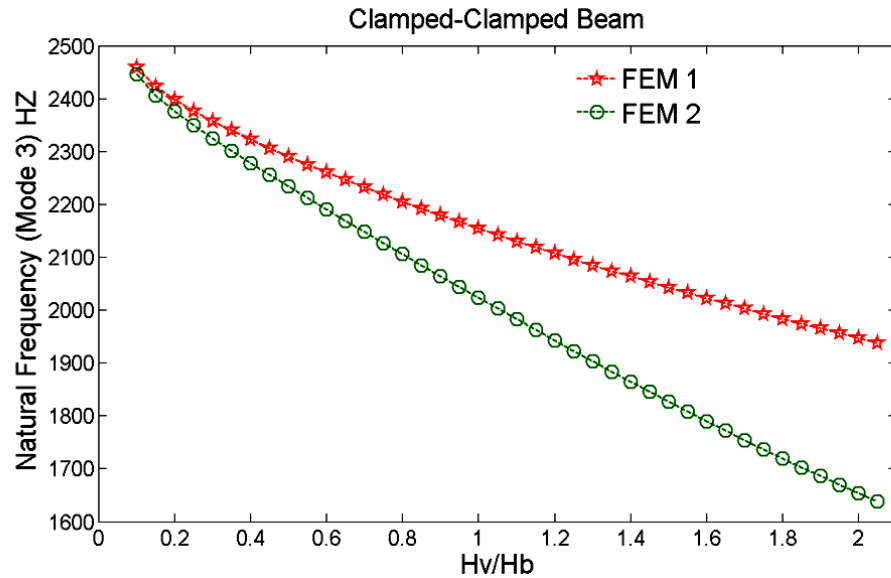
Figure 2.20 Comparison of third Natural Frequencies obtained by FEM1 and FEM2 models, by varying ratio of viscoelastic core to base layer heights for Clamped- Clamped beam
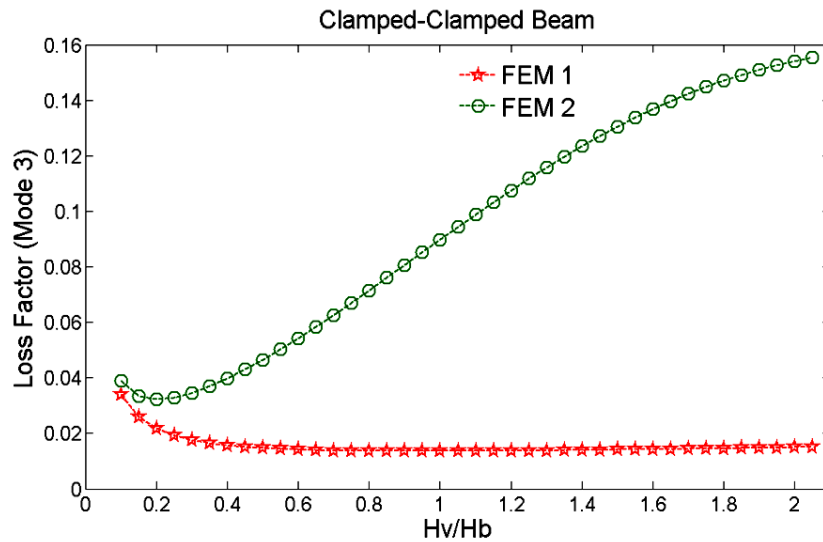
Figure 2.21 Comparison of Loss Factors (mode 3) obtained by FEM1 and FEM2 models, by varying ratio of viscoelastic core to base layer heights for Clamped- Clamped beam

As it can be realized results from both FEM models generally show a decrease in the natural frequencies and increase in loss factor with increase in thickness of viscoelastic layer. The results shows that in both clamped-free and clamped-clamped sandwich beam , for all ratios of core layer to the base layer heights, no substantial deviation exists between the first mode natural frequency and loss

factor obtained from FEM 1 and FEM 2 models. However, for the second and third mode, results based on FEM 1 and FEM 2 starts deviating with increasing the height of viscoelastic layer. This deviation is more pronounced for the loss factor. Generally, FEM 2 model tends to generate lower natural frequency and higher loss factor as compare with those based on FEM 1 model. This can be attributed due to the fact that nonlinear displacement field for the viscoelastic layer treats the viscoelastic material in less stiff way because of nonlinear terms in displacement fields and permission of compression in transverse direction. Compression damping in transverse direction leads to more heat dissipation, which is closer to the realistic behavior of viscoelastic material, thus leads to lower natural frequencies and higher loss factor as compared with linear displacement field assumption. This difference becomes more prominent for the thick viscoelastic layer at higher frequency range. This can be explained as the modulus and loss factor of the viscoelastic material is a function of frequency, thus at the higher frequency range, nonlinear terms in displacement fields become more significant. It is also interesting to note that first mode loss factor for both boundary conditions initially decreases by increasing the viscoelastic height and until reaches to a minimum value at certain viscoelastic height and then increases by increasing the viscoelastic height. For instance for the clamped-free boundary condition, the first mode loss factor becomes minimum at ratio of 0.6. This behavior is less observed for higher modes. For the second mode, the loss factor sharply decreases to its minimum values and then steadily increases and for the third mode, the loss factor is merely constant over a wide range of the viscoelastic core to base layer thickness ratios.

2.8 Conclusion

In this chapter, vibration response of a sandwich beam with a core viscoelastic layer between two layers of the continuous elastic structure has been analyzed. Mathematical modeling was developed in finite element form to simulate the dynamic response of the sandwich beam. Two different theories were implemented in the displacement field of viscoelastic layer. First theory takes linear assumption in displacement field of viscoelastic layer and the second considers higher order nonlinear displacement field in transverse and axial direction. An alternative method is presented to solve differential equation resulted from the second theory of nonlinear displacement modeling without ignoring the higher order derivatives. The validity of the both developed finite element formulation has been demonstrated by comparing the results with experimental data and other numerical model. Furthermore, it has also been demonstrated that the thickness of viscoelastic layer plays an important role in variation of natural frequencies and loss factors. It has been observed that the natural frequency at all modes decreases with increase in the thickness of the viscoelastic layer. However, the loss factor could be increased when the thickness ratio of the viscoelastic layer with the elastic base layer exceeds certain value. Further it was demonstrated, that the nonlinear assumption in viscoelastic layer displacement fields yields more accurate results than linear displacement field. The deviation between two theories becomes more as the ratio of the viscoelastic layer with the elastic base layer exceeds certain value. Difference becomes more prominent with thick viscoelastic layer at higher frequency range. This can be explained as the modulus and loss factor of the

viscoelastic material is a function of frequency, so that at higher frequency range, nonlinear terms in displacement fields become more relevant.

CHAPTER 3

3 VIBRATION ANALYSIS AND OPTIMUM DESIGN OF A PARTIALLY TREATED SANDWICH BEAM

3.1 Introduction

In view of the increased cost and weight with complete viscoelastic layer in most real-life conditions, partial damping treatment where only a portion of the base layer is covered with viscoelastic and elastic constrained layers is clearly more practical. Nokes and Nelson (Nokes, et al., 1968) were among the first investigators to present the solution of a partially covered sandwich beam. They presented the theoretical and experimental results but without conducting any optimization formulation. A more thorough analytical study for eigenvalue problem for a partially treated sandwich beam was carried out by Lall, Asnani, and Nakra (Lall, et al., 1988). They used three different approaches (two formulations based on simplified methods and one based on an exact method) to analyze the vibration and damping behavior of the beam. In the first formulation, an expression for the modal system loss factor is obtained by the ratio of energy dissipated to the maximum strain energy during a cycle in which the modes of vibration are assumed to be the same as that of the base beam. In the second formulation, they carried out the analysis by a Rayleigh-Ritz method. The assumed mode shapes satisfy the boundary conditions, leading to the complex eigenvalues defining the resonance frequencies and the associated modal system loss factors. In the third formulation, they employed the classical Euler beam theory for the uncovered portion of the beam, and the

sandwich beam theory for the covered portion, with implementing the continuity conditions at the common interface sections.

Aspiring to maximize the vibration damping of structures with minimum viscoelastic and constrained layer materials, some efforts have been also put forth to optimally design partial treatments of vibrating structures. For fully covered sandwich beams, Lifshitz and Leibowitz (Lifshitz, et al., 1987) determined the optimal layer thickness of the viscoelastic core layer.. In another optimization research by Lall, Asnani and Nakra (Lall, et al., 1987) for the partially covered plate, the objective function was to maximize the system loss factor of a specific mode, with design parameters as dimensions of the patch, and the thicknesses of constraining layer and viscoelastic layer while keeping patch coverage area constant.

In this chapter, the properties and vibration response of partially constrained layer damping (PCLD) for beam is investigated. The governing equations of PCLD treated beam are formulated using the finite element method. As it is verified in Chapter 2 that the nonlinear displacement field in viscoelastic layer is more accurate, here in this section nonlinear displacement field in viscoelastic core layer is utilized. The properties of different configurations of a PCLD treated beam are evaluated to investigate the influences of the location and length of the PCLD patch for different boundary conditions. Later in chapter, the emphasis is placed on determining the optimal location and number of patches of PCLD to maximize the modal loss factor. The loss factor correspond to the specific mode is evaluated by implementing the

energy dissipation method explained in section 2.3.9. Finally, an optimization problem is formulated and solved using the Genetic Algorithm (GA) to identify the optimum location and number of treated patches simultaneously.

3.2   Finite Element Modeling of a Partially Treated Beam

A partially-treated sandwich beam can be modeled on the basis of finite element models developed for a fully treated beam. The beam structure with multiple patches of constrained layer treatment can be modeled by treating each patch independently and then coupling with the adjacent segment to assure compatible deformation and continuous response of the composite structure. This could be achieved by imposing compatibility conditions which are identical displacements and the slopes at the boundaries of the adjacent segments. For the sake of simplicity, the length of the segment treated or untreated is constrained by the length of the single element in the finite element model. Thus to vary the length of the treated area, we have to add an adjacent element as treated element or untreated element. Therefore two kinds of element matrices are developed for both mass and stiffness matrices.   The development of the element matrix for the treated part using nonlinear displacement field at core viscoelastic core layer is thoroughly explained in section 2.4. In this section we discuss about the development of element matrix for the untreated part of beam, which is the bare base beam.

The displacement fields for bare base beam have already been discussed in section 2.3.2 and provided in Eq. (2.1) and Eq. (2.2) for axial and transverse directions.

Considering this, the generalized degrees of freedom for bare beam in analytical form can be written as:

$$q = \begin{bmatrix} u_b^0 & \theta_b & w^0 \end{bmatrix}'$$ (3.1)

The expression for normal and shear strains for the bare base beam is expressed in Eq. (2.14). The Strain and kinetic energy for the bare base beam can also be evaluated by the expression expressed in Eqs (2.19) and (2.22), respectively.

The finite element formulation of the bare beam is explained in this section. The proposed element has three nodes and considering the generalized degrees of freedom given in Eq. (3.1), each node has three nodal displacement degrees of freedom as shown in Figure (3.1).
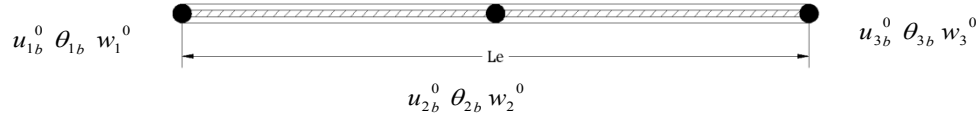
Figure 3.1 Three-node beam element having three degrees of freedom per node

The generalized degrees of freedom q are related to the elementary nodal degrees of freedom q_e through the shape function matrix N as:

$$q = N q_e$$ (3.2)

$$q_e = \begin{bmatrix} u_{1b}^0 & \theta_{1b} & w_1^0 & u_{2b}^0 & \theta_{2b} & w_2^0 & u_{3b}^0 & \theta_{3b} & w_3^0 \end{bmatrix}'$$ (3.3)

$$N = \begin{bmatrix} N_1 & 0 & 0 & N_1 & 0 & 0 & N_1 & 0 & 0 \\ 0 & N_2 & 0 & 0 & N_2 & 0 & 0 & N_2 & 0 \\ 0 & 0 & N_3 & 0 & 0 & N_3 & 0 & 0 & N_3 \end{bmatrix}$$ (3.4)

The interpolation functions are similar to those in Eqs (2.28)-(2.30). Equations of motion for the element can be formulated using the Hamilton's principle expressed

in Eq. (2.31). Now by substituting the expression for the kinetic energy, strain energy and work done and integrating over the time, we obtain:

$$[M_{be}]\{\ddot{q}_e\} + [K_{be}]\{q_e\} = 0 \tag{3.5}$$

where M_{be} and K_{be} are the mass and stiffness matrices of an element for the bare beam, respectively.

Now, mass and stiffness matrix of treated beam and bare beam in Eq. (3.5) are assembled accordingly to obtain the mass and stiffness matrix of the partially treated beam. As discussed in section (2.4.5) the equations can be solved by the same technique for harmonic loading and free vibration.

3.3 Parametric Studies

The properties of a partially treated sandwich beam are strongly influenced by the number, size and location of the treated segments. Here in this study, the finite element model formulated in section 3.2 is used to investigate the effects of variations in the location and length of the treated segments of the beam on the natural frequencies and loss factor under different boundary conditions. The height (thickness) of all the three layers is kept constant. The base and top constrained layers are made of Aluminum and the core layer is made of viscoelastic material Neoprene CR-602 which is similar to that chosen by Leibowitz & J.M (Leibowitz, et al., 1990) in their experiment (Leibowitz, et al., 1990). The mechanical properties of the materials are discussed in section 2.5. The total length of the multi-layer beam is divided into 18 segments of equal length. The geometric dimension of layers for sandwich beam is provided in Table 3.1.

Table 3.1 Geometric dimension of partially treated sandwich beams

Geometric Dimension of Sandwich beams for parametric studies		
Specification	Clamped-Free Beam	Clamped-Clamped Beam
(Length of Beam) L (mm)	180	180
(Width of Beam) D (mm)	15	15
(Height of base layer) H_b (mm)	5	5
(Height of top constrained layer) H_t (mm)	2.5	2.5
(Height of viscoelastic core layer) H_v (mm)	5	5

Three different cases for parametric studies have been investigated for both the clamped-free and clamped-clamped boundary conditions. In the first case, length of 50mm on beam is kept bare, which is equal to the length of 5 elements and rest of the length is treated with the viscoelastic core and top constrained layers. Position of this cut in is varied from the left clamped side of clamped-free and clamped-clamped beam. Influence of the position of the cut on the natural frequency and loss factor for the first vibration mode is investigated. In the second case, only 50 mm of the length of beam is treated with the viscoelastic core and top constrained layers and rest of the area is kept bare. Position of this treated patch is also varied from the left clamped side of clamped-free and clamped-clamped beam to investigate the effect of the position of patch on the natural frequency and loss factor for the first vibration mode. Finally for the last case, the length of the treated patch is increased further keeping the patch position fixed at left clamped side of clamped-free and clamped-clamped beam until it cover the whole length of the beam. The objective in this case is to examine the effect of the length of patch on the natural frequency and loss factor for the first mode.

3.3.1 Effect of location of the cut on the natural frequency and loss factor (Case 1)

Position of cut is defined from the clamped left side of the clamped-free and clamped-clamped beam. The length of the cut as discussed earlier is 50 mm and is kept constant in this case. Figure (3.2) illustrates the discretized model of beam, which is partially treated with a viscoelastic core and top constrained layers.
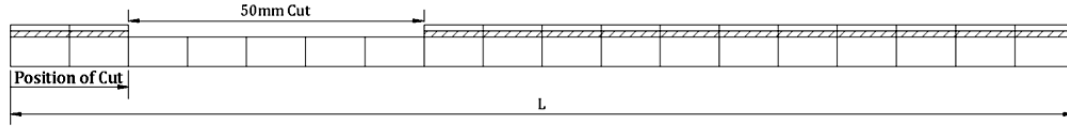
Figure 3.2 Discretized model of partially treated beam with a cut in core and constrained layers

The position of cut is varied from the left clamped side of both clamped-free and clamped-clamped beam, initially at the extreme left end and then shifting towards the right side, till the right side of the cut reaches the extreme right side of beam, which in case of clamped-free beam is free side.

The natural frequency and loss factor of the first vibration mode is evaluated as the position of cut shifts towards right by one element each time. Both the natural frequency and loss factor as shown in Figures (3.3) and (3.4) respectively, increases as the position of cut gradually moves towards the free side of clamped-free beam. Basically placing the cut at the vicinity of the cantilever end will separate the viscoelastic treated part from the cantilever end. This will cause maximum reduction in the stress induced in the viscoelastic treated part and subsequently maximum reduction in natural frequency and loss factor of the sandwich beam. As the cut moves forward to the free end, the effect of stress reduction due to introduction of the cut would be less and thus causing increase in natural frequency and loss factor.

81

In the case clamped-clamped beam, the natural frequency and loss factor as shown in Figures (3.5) and (3.6) respectively, increases and become maximum as the position of cut reaches to the center of the beam and symmetrically decrease as the position of cut moves further towards the other end, which is expected due to the symmetric nature of boundary condition in clamped-clamped beam. The above results evidently demonstrate the sensitivity and importance of position of cut to optimize the stiffness and damping of the sandwich structure.
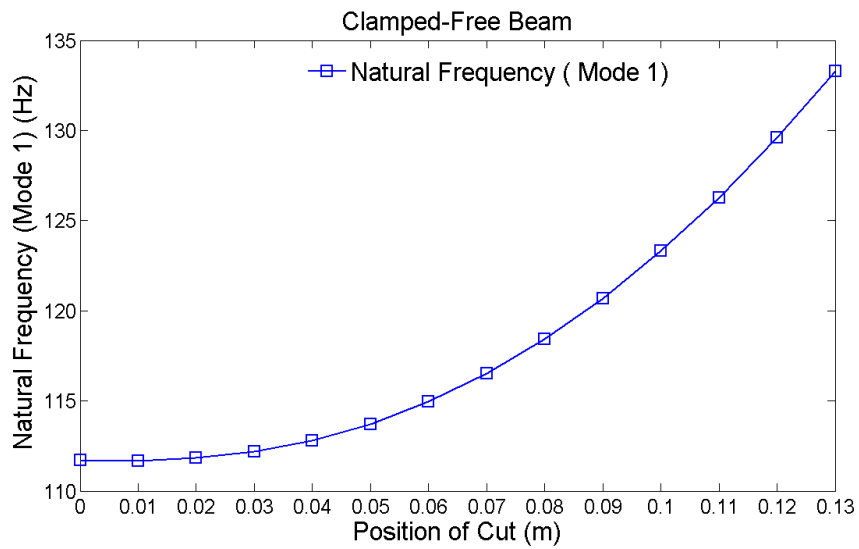
Figure 3.3 Variation of first natural frequency with position of cut in partially treated clamped-free beam
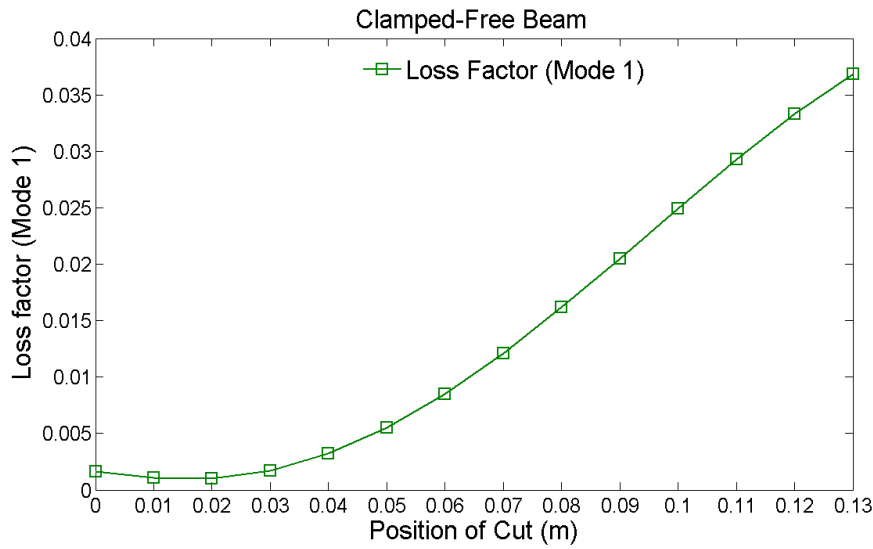
Figure 3.4 Variation of Loss factor (Mode 1) with position of cut in partially treated clamped-free beam
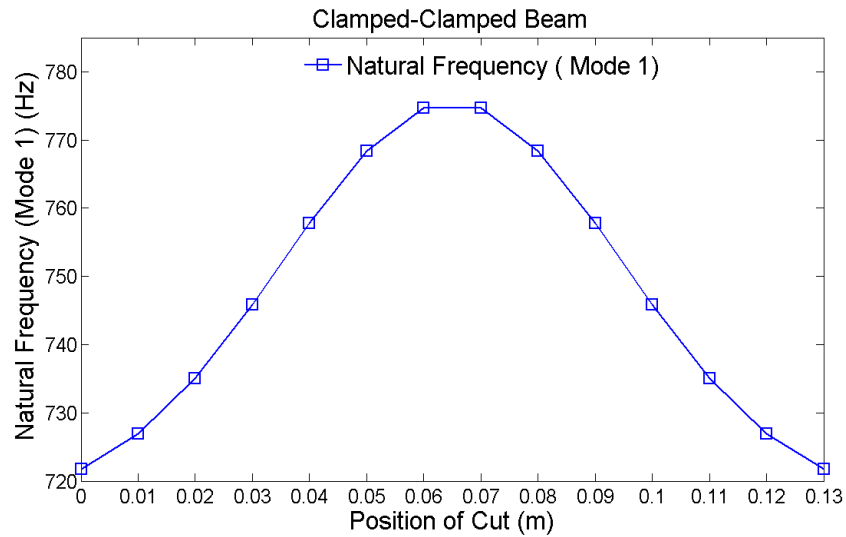
Figure 3.5 Variation of first natural frequency with position of cut in partially treated clamped-clamped beam
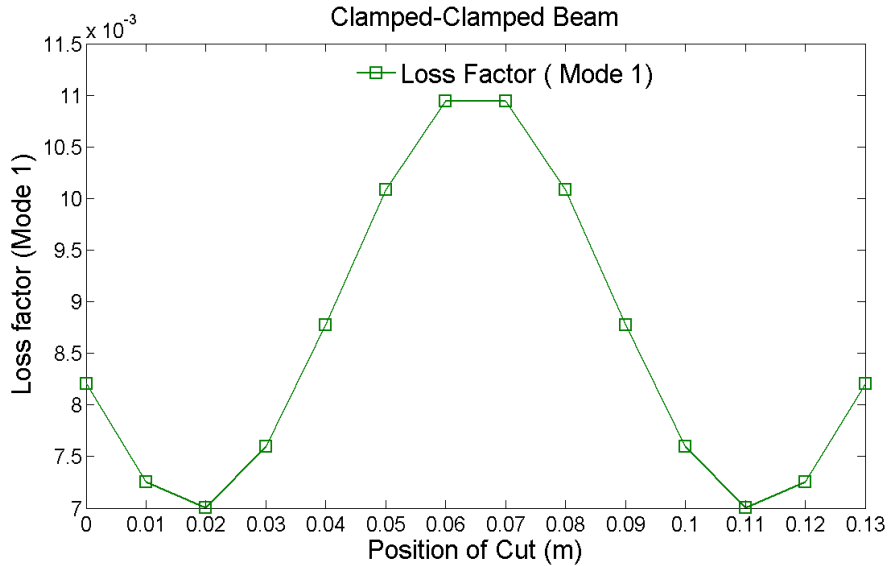
Figure 3.6 Variation of Loss factor (Mode 1) with position of cut in partially treated clamped-clamped beam

3.3.2 Effect of the location of treated patch on the natural frequency and loss factor (Case 2)

Position of the patch is defined from the clamped left side of the clamped-free and clamped-clamped beam. The length of the patch as discussed earlier is 50 mm and is kept constant in this case. Figure (3.7) illustrates the discretized model of beam, which is partially treated with a viscoelastic core and top constrained layers.
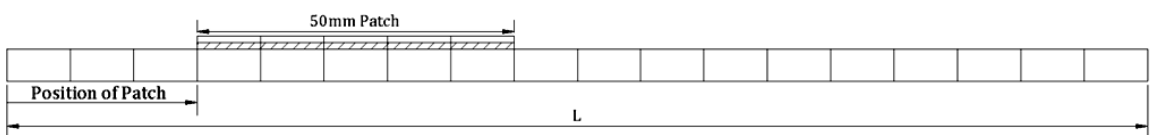
Figure 3.7 Discretized model of partially treated beam with a patch of core and constrained layers

The position of the patch is varied from the left clamped side of both clamped-free and clamped-clamped beam, initially at the extreme left end and then shifting towards the right side, till the right side of the patch reaches the extreme right side of beam.

Similar to the Case 1, the natural frequency and loss factor of the first vibration mode is evaluated as the position of patch shifts towards right by one element each time, for both boundary conditions. Results for natural frequency and loss factor for the cantilever-free sandwich beam are shown in Figures (3.8) and (3.9), respectively. As it can be realized, both natural frequency and loss factor decreases as the position of cut gradually moves towards the free side of clamped-free beam. It should also be noted that there is a drastic reduction in the loss factor once the patch is separated from the cantilever end and then decreases steadily as the patch moves towards the free end. As discussed before this can be attributed to the fact that when the patch is separated from the cantilever end, then it becomes free from both sides which significantly reduces the stress induced in the patch.

For the clamped-clamped beam, results for natural frequency and loss factor are shown in Figures (3.10) and (3.11), respectively. It can be seen that, natural frequency and loss factor are maximum at the fixed ends and then decreases symmetrically as the position of patch moves towards the center. It should be noted that for the clamped-clamped condition, the loss factor start increasing slightly, after the initial sharp reduction, as the patch moves toward the center of the beam. This can be attributed to the fact that beam bends in symmetric form and at the centre of the beam rotational degree of freedom is negligible which act as induced boundary condition and induce shear stress either sides of it. The above results again exhibit the significance of position of patch to optimize the stiffness and damping of structure.
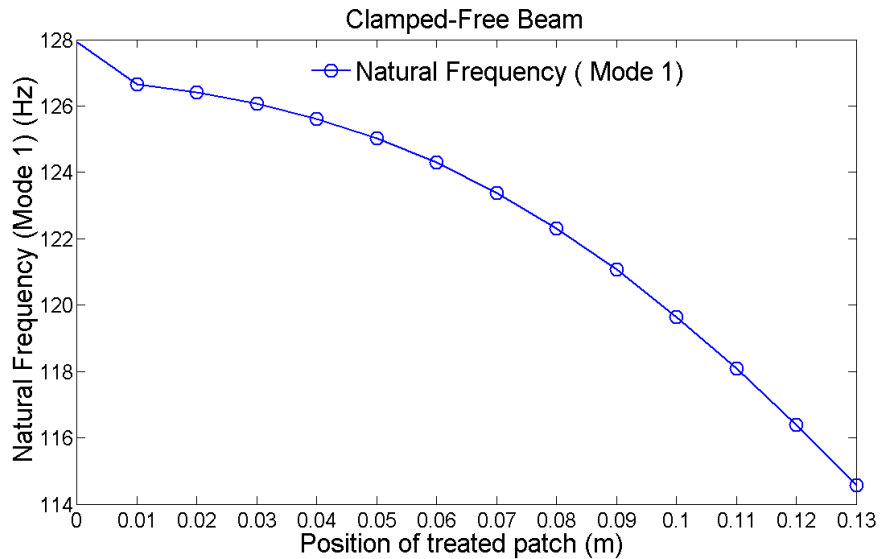
Figure 3.8 Variation of first natural frequency with position of treated patch in partially treated clamped-free beam
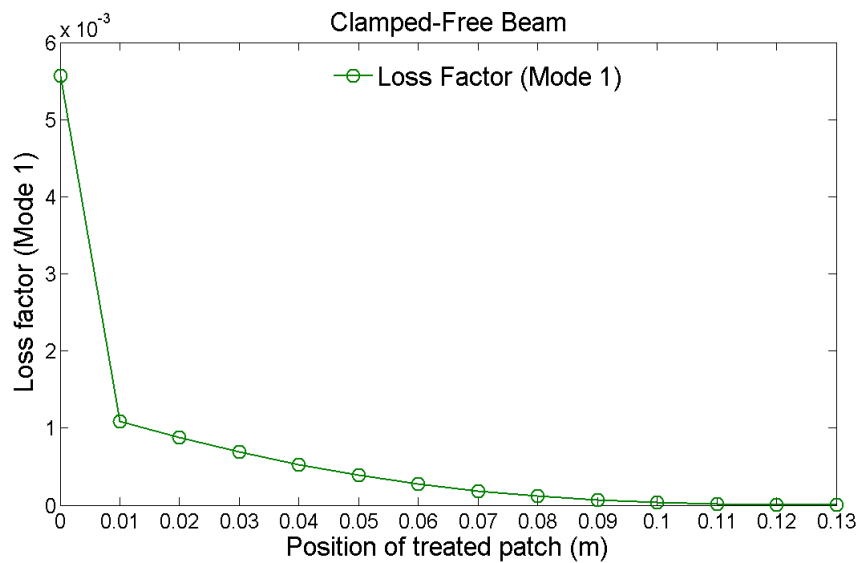
Figure 3.9 Variation of Loss factor (Mode 1) with position of treated patch in partially treated clamped-free beam
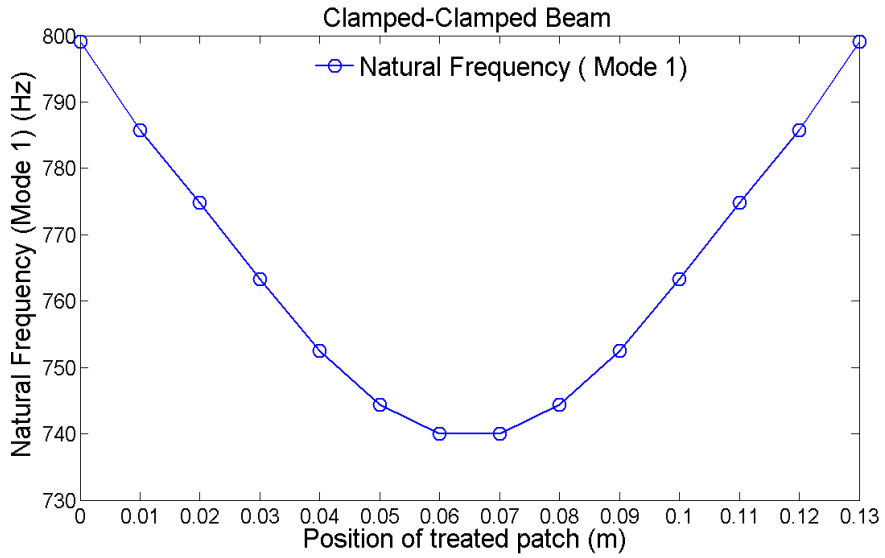
Figure 3.10 Variation of first natural frequency with position of treated patch in partially treated clamped-clamped beam
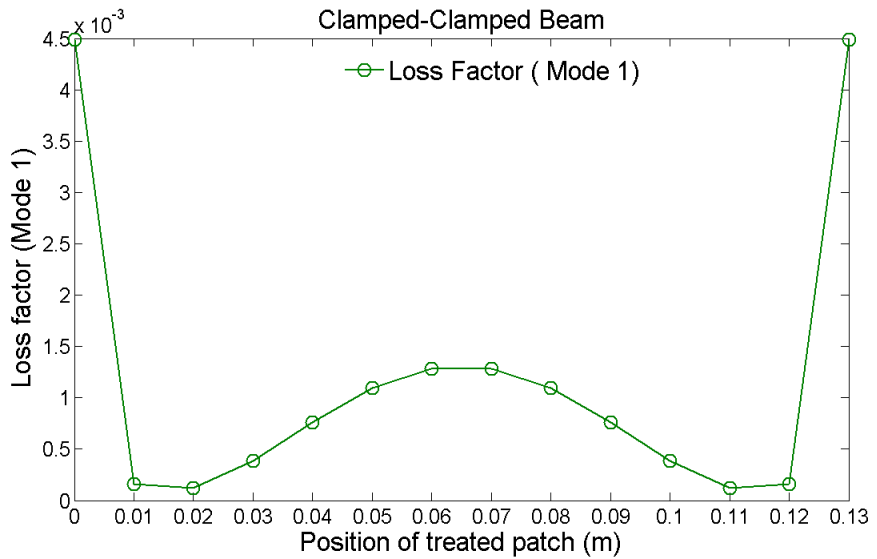
Figure 3.11 Variation of Loss factor (Mode 1) with position of treated patch in partially treated clamped-clamped beam

3.3.3 The effect of length of the patch on natural frequency and loss factor (Case 3)

Length of the patch is defined from the clamped left side of the clamped-free and clamped-clamped beam. The initial length of the patch as discussed earlier is 50 mm and increased towards the extreme right side gradually by one element length at each time. Figure (3.12) illustrates the discretized model of beam, which is partially treated with a viscoelastic core and top constrained layers.

87
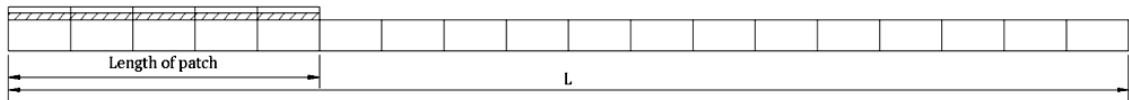
Figure 3.12 Discretized model of partially treated beam with varying patch length of core and constrained layers

The natural frequency and loss factor of the first vibration mode is evaluated as the length of patch increases towards right side by one element each time, for both end conditions. The results for the natural frequency and loss factor for the clamped-free beam are shown in Figures (3.13) and (3.14). The result shows that the natural frequency initially increases as the length of patch increases, but after certain length (around 10 mm) the natural frequency decreases as the length of patch increases. This may be due to the fact that the further increase in patch length does not augment stiffness, as the free side of clamped-free undergoes less stress relative to the fixed end, but the mass of the system is increasing at the same rate, thus leading to decrease in natural frequency. But the loss factor as shown in Figure (3.14) increases gradually with increase in the patch length. For the case of clamped-clamped beam, the results for natural frequency and loss factor are shown in Figures (3.15) and (3.16), respectively. As it can be realized, here for the case of clamped-clamped boundary condition, natural frequency decreases as the length of patch increases until it reaches to its minimum value at the length of about 160 mm. However, the loss factor generally increases by increasing the patch length while experiencing one local maxima and minima in the given range.
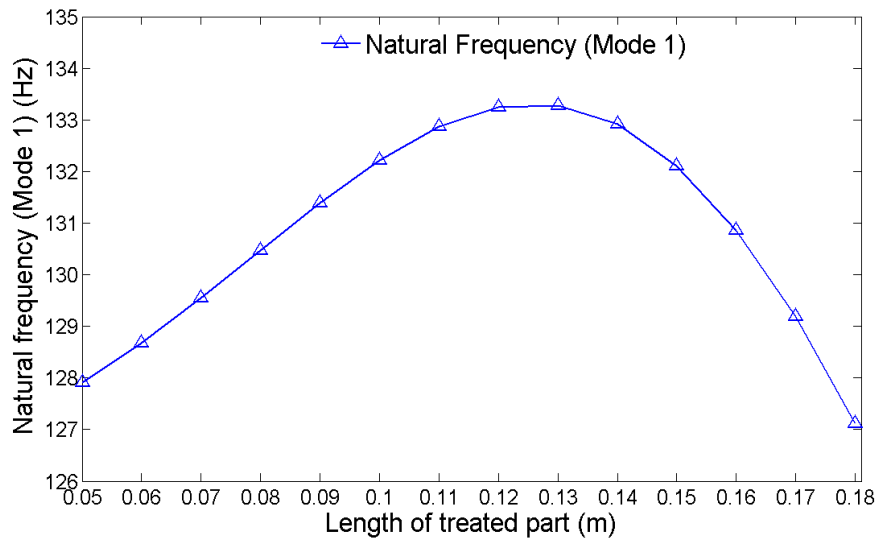
Figure 3.13 Variation of first natural frequency by varying the length of treated patch in partially treated clamped-free beam
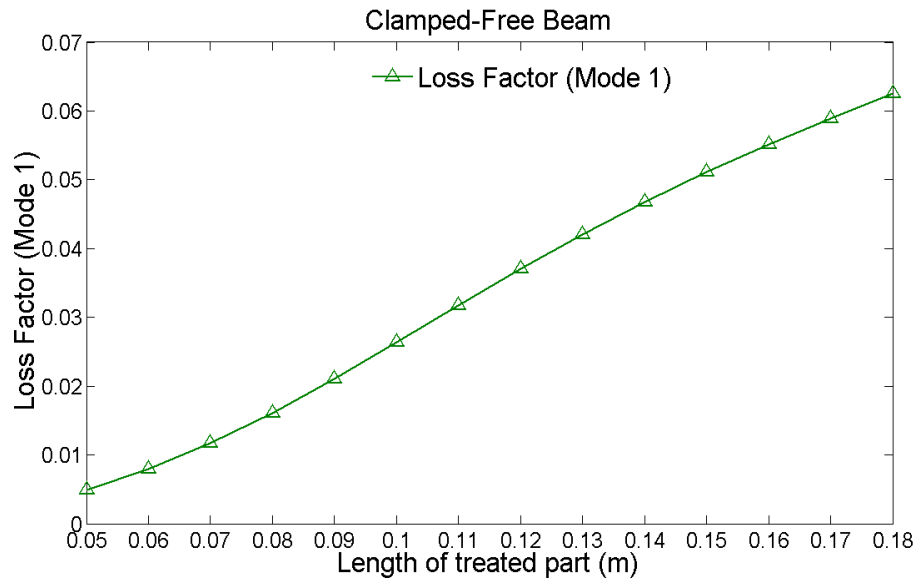
Figure 3.14 Variation of Loss factor (Mode 1) by varying the length of treated patch in partially treated clamped-free beam
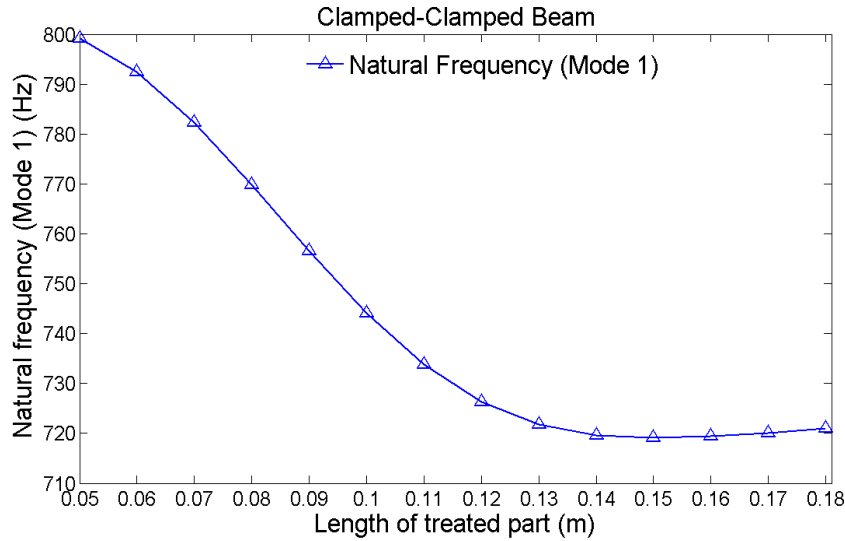
Figure 3.15 Variation of first natural frequency by varying the length of treated patch in partially treated clamped-clamped beam
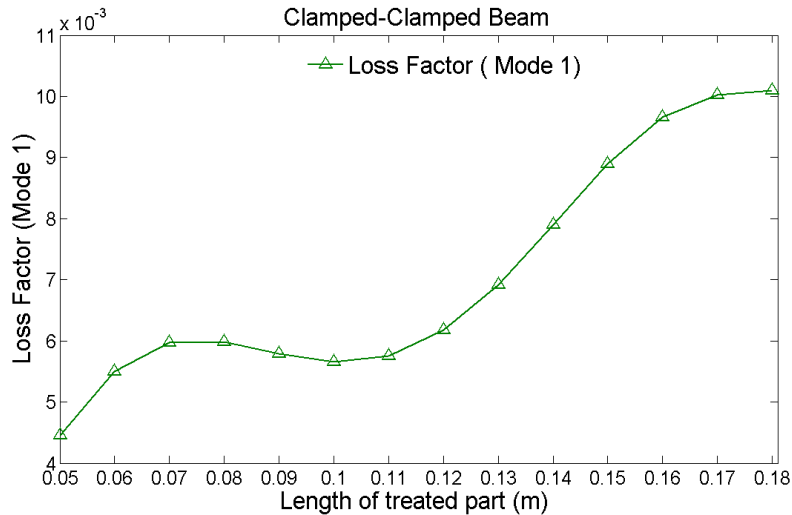
Figure 3.16 Variation of Loss factor (Mode 1) by varying the length of treated patch in partially treated clamped-clamped beam

3.4 Formulation of the optimization problem

Previous parametric studies demonstrated that in order to design a partially treated sandwich beam, it is necessary to obtain an appropriate layout of a structure so that it yields the maximum shear energy distribution resulting in maximum modal loss factor. As discussed in section 3.3, it becomes evident that the location and size of

patches and cuts considerably affect he natural frequency and modal loss factor. Thus, it is essential to optimize the number and location of segments treated and untreated in order to maximize the modal loss factor with minimum possible increase in the weight of structure. In this study, an optimization problem is formulated for the partially treated sandwich beam with viscoelastic and constrained layers to achieve maximum modal damping factor corresponding to the first vibration mode. The problem is formulated for two different end conditions namely clamped-free and clamped-clamped boundary conditions, while the height (thickness) of both core viscoelastic and top constrained layers kept constant. Similar to that in previous section 3.3, the base and top constrained layers are made of Aluminum and the core layer is made of viscoelastic Neoprene CR-602 same as that chosen by Leibowitz & J.M. (Leibowitz, et al., 1990) in their experiment. (Leibowitz, et al., 1990) The mechanical properties of the materials are discussed in section 2.5. Also, the total length of the multi-layer beam is divided into 18 segments of equal length. The geometric dimension of layers for sandwich beam is provided in Table 3.1. The optimal locations and numbers of the elements to be treated are sought for two different cases. The objective here is to maximize the modal loss factor related to the first vibration mode. The loss factor for the first mode is calculated by the method described in section 2.5 in Eq. (2.66) as:

$$LF_m = f(X(n, p_n)) = \frac{\psi_m' K_m'' \psi_m}{\psi_m' K_m' \psi_m} \qquad m = 1$$

$$\text{Subject to: } 0 < n < N$$

where m is the mode number , n is the number of treated elements, and p_n is the

location number of the treated elements associated to the finite element model of

total N elements. The matrix X defines as the number and the locations of the

treated patch along the beam length based on the element segment number. This

has been done by the binary numbers, in which zero is regarded as the untreated

element and one is for the treated element.

3.5   Optimization Method and results

 The optimization problem defined in section 3.4 is solved to identify the global

optimum locations and numbers of treated segments. A number of optimization

algorithms are available to seek solutions of such types of problem. The vast

majority of the gradient-based optimization algorithms tend to easily converge to

the local optima. Alternatively, non-gradient stochastic search algorithms such as

Genetic Algorithms (GAs) may be used to locate the global optimum point with

reasonable accuracy in a more efficient manner (Muc, et al., 2001). Here, the

optimization problem has been solved using the GA available in the MATLAB

optimization toolbox. The results are obtained for two cases of clamped-free and

clamped-clamped boundary conditions. Table 3.2 provides the optimal numbers

and locations of the treated elements together with the optimal modal loss factor

and natural frequency for the first vibration mode derived from the GA technique.

Table 3.2 Optimum number and location and values for Loss factor and natural frequency

Optimum number and location and values for Loss factor and natural frequency				
Boundary Conditions	Number	Location	Loss Factor	Natural Frequency (Hz)
Clamped-Free	18	1 2 3 4 5 6 7 8 9 10 11 12 13 14 15 16 17 18	0.0625	110.34
Clamped-Clamped	15	1 2 3 4 5 6 7 8 9 10 11 12 13 14 15 16 17 18	0.0106	679.85
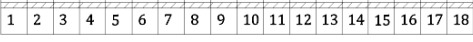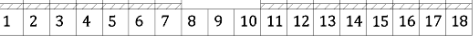
It can be realized that for the case of clamped-free beam, the maximum loss factor is achieved when the whole beam is covered by the constrained viscoelastic layer (fully treated viscoelastic beam). However for the case of clamped-clamped boundary condition, the maximum loss factor occurs when the treated elements are mainly clustered at the end points (partially treated viscoelastic beam).

3.6   Conclusion

In this chapter, the damping performance of a partially treated sandwich beam was studied in terms of the modal loss factor and natural frequency. First, the modal loss factor and natural frequency corresponding to the first vibration mode of the partially treated sandwich beam have been evaluated using the finite element model developed for a partially treated sandwich beam. The effect of location of the cut in viscoelastic and constrained layers of a partially treated sandwich beam on the first modal damping factor is demonstrated under different end conditions. It was shown that the location of cut plays an important role on the variation of the modal damping factor irrespective of the end conditions. It was also concluded that the clamped-free and clamped-clamped end conditions yield the highest and lowest modal damping factors respectively among the end conditions considered

irrespective of the mode of vibration. It is also verified that location and length of treated patch have great influence on the both natural frequency and modal loss factor. Then a design optimization methodology to maximize the modal loss factor with minimum possible number of treated segments for first vibration mode has been formulated by combining the developed finite element analysis and optimization algorithms based on Genetic Algorithm. It is shown that for the clamped-free end condition, all the segments must be treated with viscoelastic and constrained layers in order to achieve maximum loss factor, but for the clamped-clamped end condition, it is proved that partially treated beam leads to greater damping behavior than fully treated beam. This leads to the reduction of the weight of structure.

CHAPTER 4

4 THERMAL ANALYSIS OF SANDWICH BEAM UNDER HARMONIC LOAD

4.1 Introduction

We have discussed earlier that, mechanical and damping properties of viscoelastic material are not only function of the excitation frequency but also function of the temperature. In the chapter, we will account the effect of heat generation on the properties of viscoelastic core layer while the sandwich beam structure undergoes harmonic loading. The effect of temperature developed is observed on the material properties like modulus and loss factor of viscoelastic layer. Later the result of variation in material properties is observed on the transverse response of beam. Energy dissipation due to the cyclic loading discussed earlier in section (1.4.4) leads to generation of heat. This heat is generated within the viscoelastic core and varies with strain developed in the viscoelastic core material along the axial direction of the sandwich beam. As the viscoelastic materials are also known for their heat insulation properties, thus the heat generated might not readily transfer to the environment from the top and bottom faces of elastic layers by convection after conducting through the thickness of base and top layers. As a result, the spatial variation of the temperature occurs in transverse and axial direction across all the layers with time. So the complex shear modulus of the viscoelastic core needs to be updated incrementally after each cycle. The temperature rise in elastic top and base layers has negligible effect on their mechanical properties as it is not high enough.

But as the viscoelastic material is very sensitive to small change in temperature, thus the effect of temperature cannot be ignored. The temperature rise within the viscoelastic material shows its effect in *G'(ω,T)* and *G''(ω,T)* by replacing the *T* by *T+ΔT* (Soong, et al., 1997) . The dissipated energy discussed in Eq. (1.68) can be utilized to calculate the energy dissipated in each element of the finite element model (FEM) and can be written as

$$D_e = \pi \{q_e\}' [K_e''(\omega)] \{q_e\}$$ (4.1)

where D_e is the energy dissipated from an element. By replacing the associated nodal displacement values for each element in Eq. (4.1), the value of D_e is evaluated for each element of the viscoelastic layer. The obtained dissipated energy from FEM model is then used as an input heat in the relative heat transfer equation to obtain the transient temperature developed in all layers.

4.2   Central Finite Difference Model

Each layer of sandwich structure within a single element of FEM is divided into seven rectangular cells along the axial direction and two cells in thickness. Vertices of rectangular cells are considered nodes. Moreover to consider the heat transfer through convection to environment and isolated boundaries additional cells are introduced at the boundaries. As the heights of each layer are different and length of cell in axial direction is fixed, finite difference formulation using irregular grid has been employed as shown in Figure (4.1). The heat transfer along width direction is ignored due to small amount of the heat which is transferred directly to the

environment by convection through the small area of the lateral sides of the sandwich structure.
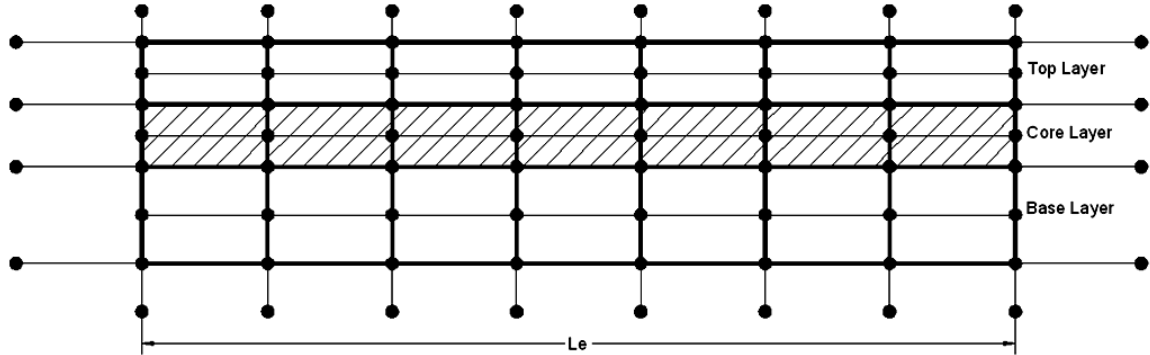
Figure 4.1 Finite difference model of Sandwich Beam

4.3 Heat Equation

Here the finite difference model discussed in previous section is used to derive the heat transfer equation. Each node in the model represents a region called a control volume as shown in Figure (4.2).
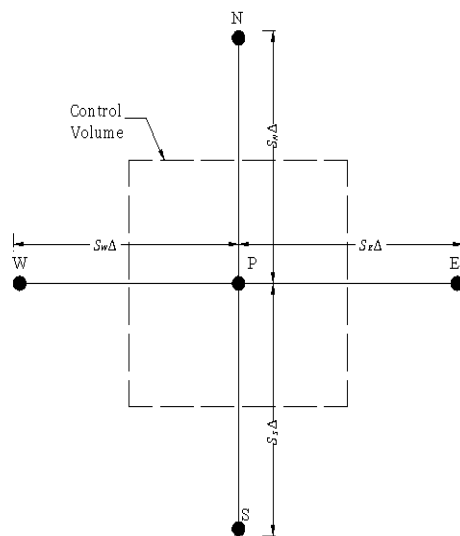
Figure 4.2 Cell Control Volume around a typical node P in 2-D coordinate

Energy balance method is considered to derive the equation of heat transfer. According to this principle, summation of the net rate of heat flow that enters the

control volume by conduction through each surface of the control volume and the rate of generated heat inside the control volume should be in equilibrium with the rate of increase of internal energy of the control volume. These energies can be described as:

Rate of heat flow from node N to P
$$Q_{NP} = k_{NP} \frac{V}{\frac{\Delta}{2}(S_N + S_S)} \frac{T_N - T_P}{S_N \Delta} \tag{4.2}$$

Rate of heat flow from node S to P
$$Q_{SP} = k_{SP} \frac{V}{\frac{\Delta}{2}(S_N + S_S)} \frac{T_S - T_P}{S_S \Delta} \tag{4.3}$$

Rate of heat flow from node E to P
$$Q_{EP} = k_{EP} \frac{V}{\frac{\Delta}{2}(S_E + S_W)} \frac{T_E - T_P}{S_E \Delta} \tag{4.4}$$

Rate of heat flow from node W to P
$$Q_{WP} = k_{WP} \frac{V}{\frac{\Delta}{2}(S_E + S_W)} \frac{T_W - T_P}{S_W \Delta} \tag{4.5}$$

Rate of the internal heat generated in the control volume
$$HV \tag{4.6}$$

Rate of increase of internal energy of the control volume
$$(\rho C_P)_{eff} V \left(\frac{\Delta T}{\Delta t} \right) \tag{4.7}$$

in which k is the conductivity between different nodes, V is the control volume, S_S, S_N, S_E, S_W, S_I and S_O are non-dimensional ratios to represent the spacing between the point P to N, S, E, W, I and O, according to the reference value of Δ as shown in Figure 4.2, where point I and O are points normal to paper inside and outside directions, which represent the lateral direction of the sandwich beam and H is the rate of generated heat per unit of volume. Δ is arbitrary value and here is considered to be the height of the base layer. C_P is specific heat, ρ is density and $\Delta T/\Delta t$ is the

rate of rise in temperature. Since the material properties inside the control volume are not uniform, an effective $(\rho C_P)_{eff}$ should be used in each finite difference equation. The detail process of deriving above described energy terms is described in Appendix B. After manipulating the above energy terms, the transient finite difference equation for node P can be written as:

$$k_{NP} \frac{T_N - T_P}{S_N(S_N + S_S)} + k_{SP} \frac{T_S - T_P}{S_S(S_N + S_S)} + k_{WP} \frac{T_W - T_P}{S_W(S_E + S_W)} + k_{EP} \frac{T_E - T_P}{S_E(S_E + S_W)}$$
$$+ H = \frac{(\rho C_P)_{eff} \Delta^2}{2} \left(\frac{\Delta T}{\Delta t} \right) \tag{4.8}$$

After assembling the equations for all nodes and applying the boundary conditions for clamped-clamped beam (convection at the top and bottom of the beam and isolation at the end sides), the unknown temperature at the left side of the Eq. (4. 8) can be determined according to the known temperature at the right side trough the implicit method during each increment Δt. The dissipated energy per unit volume defined in Eq. (4.1) can be substituted into the Eq. (4.8) for H after each cycle. The material properties of the viscoelastic layer now are updated according to the new state of the temperature at each element which is the average values calculated from the seven cells of viscoelastic layer in finite difference model.

4.4 Numerical Result and Validation of the Finite Difference Model

This section presents validation case for the presented finite difference model for sandwich beam. Total 114 cells are used in axial direction and 7 cells in transverse direction to cover all the three layers to represent the finite difference model of sandwich beam. The Finite difference model referred here as FDM. The model is

validated by the numerical results generated using the ANSYS model of composite beam of three layers similar to the sandwich beam (referred as ANSYS). It is assumed that all three layers are initially at temperature 0 °C and then temperature of the base layer is suddenly increased to 40 °C and kept constant along the length while the top elastic layer is maintained at 0 °C along the length. The temperature at two points is observed transiently, one in the middle of the viscoelastic core layer height and second at the middle of the top layer height at the center of the beam.

The length and width of the sandwich beam is considered to be 1m and 30 mm, respectively. The height of all three layers is provided in Table 4.1.

Table 4.1 Geometric Configuration of beam for thermal analysis

Beam	H_b (mm)	H_v/H_b	H_t/H_b
Clamped-Clamped	10	0.5	0.5

The viscoelastic layer is made of a Viton-B and top and base layers are made of 2024 Aluminum layers. The Young's modulus E= 71 GPa and density 2766 Kg/m^3 is used for Aluminum layers. The density of Neoprene is taken as 1050 Kg/m^3 and dynamic properties of the viscoelastic core provided in (Nashif, et al., 1985) are given in Figures (1.14a), (1.14b) and (1.15). Figure (4.3) shows the transient temperature at the selected points evaluated by the developed FDM model and that of ANSYS model. As it can be realized, excellent agreement exists between two models confirming the accuracy of the developed FDM model for the further study.
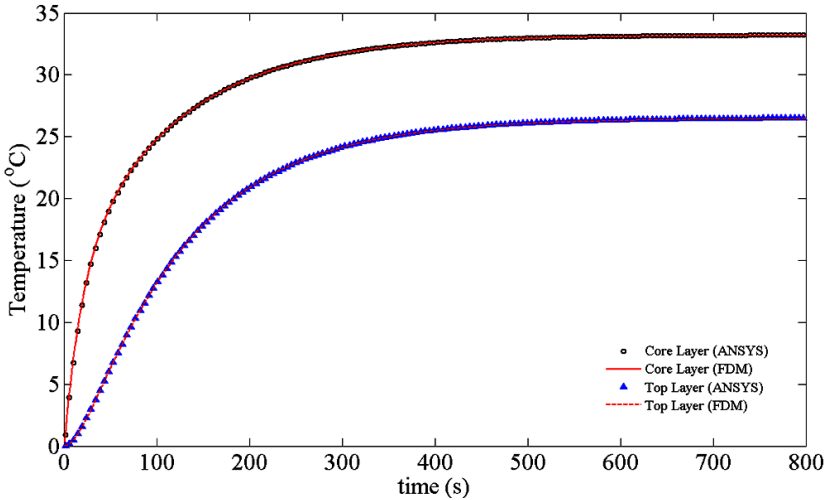
Figure 4.3 Validation of FDM model with ANSYS numerical model for transient Temperature

4.5 Thermal Analysis

Having established confidence in the FDM model for calculating the transient temperature, we can now investigate the effect of temperature increase due the generated heat in vibration response of the fully treated clamped-clamped sandwich beam under harmonic loading excitation. The configuration of the beam is the same as that in previous section. The beam is excited with harmonic load with amplitude of 100N and excitation frequency of 45 Hz at the center of the beam in transverse direction. The initial temperature of the structure is that of environment, which in this case is assumed to be 23°C. The variation in temperature developed in viscoelastic layer and transverse response are evaluated over a period of time and the results are shown in Figures 4.4 and 4.5, respectively. As, we can observe the large variation of temperature along the length, which can be attributed the variation of shear stress developed in core layer and to the fact that viscoelastic material has low heat conductivity, so, heat generated accumulate in specific areas. The transverse response at the mid-span of the beam shown in Figure 4.5 elevates

101

over the period of time, this shows the importance of considering the temperature developed in viscoelastic layer. As we can observe that, the areas where temperature is developed are away from the mid-span, but still there is rise in response, this proves the fact that overall damping of the system has been reduced.
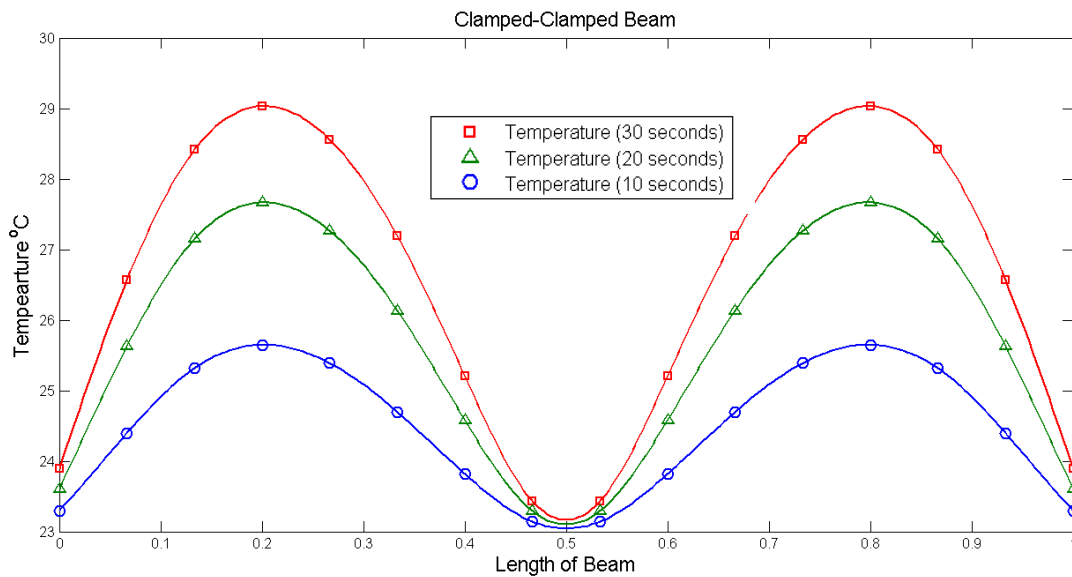
Figure 4.4 Temperature gradient developed long the length of beam in viscoelastic layer over the time
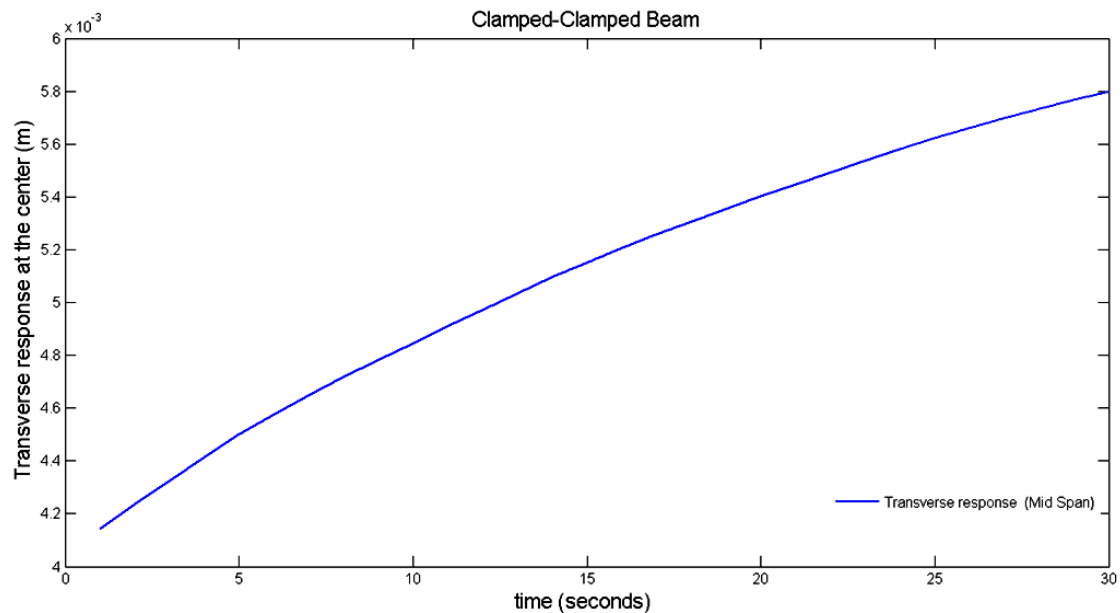
Figure 4.5 Variation in transverse response at mid- span of beam over the time

4.6 Conclusion

In this chapter, the damping performance of fully treated sandwich beam with clamped-clamped boundary condition under steady state harmonic load at the mid span is evaluated, while considering the effect of internal heat generation in the viscoelastic material. A finite difference model has been developed to evaluate the transient temperature in sandwich layers. It is shown that the temperature gradient is developed within the viscoelastic layer over the time. Further, it is demonstrated that damping performance of structure is reduced due the internal generated heat which subsequently causes the transverse response at the mid span of beam to increase over the time.

CHAPTER 5

5 CONTRIBUTIONS, CONCLUSIONS AND FUTURE RECOMMENDATIONS

5.1 Major Contributions

This dissertation research is focused on the damping potentials of structures treated either fully or partially by viscoelastic material with constrained layer on top. Analytical and experimental studies have already been contributed to the understanding of vibration suppression capabilities of the viscoelastic treated sandwich beams and the effectiveness of the partially treated sandwich structure on vibration control. However, very few studies have been done on the significance of nonlinear displacement fields that lead to higher order shear stress theory in the sandwich core layer. Furthermore, the study of internal heat generation in the viscoelastic layer has been, confined to very few cases that are only in the pure shear modes. The effects of internal heat generation on the viscoelastic material and its damping properties in a sandwich structure haves not yet been explored theoretically. A comprehensive research has been carried on the effectiveness of the partially treated structures compared to the fully treated structures. The foremost contributions of the dissertation research are summarized below:

    i.   A numerical model of a fully treated viscoelastic sandwich beam using the finite-element method with linear displacement field at core is formulated. Theoretical investigation on the dynamic characteristics of the viscoelastic sandwich beam with different boundary conditions has been carried out.

ii. Formulation of a numerical model of a fully treated viscoelastic sandwich beam using the finite-element method with nonlinear displacement field at core and the development of an alternative method to solve the governing differential equations resulted from the nonlinear modeling without ignoring the higher order derivatives have been done.

iii. Comprehensive study of the linear and nonlinear model assumptions of displacement fields at core is done and the deviation between two theories by varying the thickness of core layer for different modes is demonstrated.

iv. Numerical models of a partially treated viscoelastic sandwich beam with different end conditions are developed and investigation on its dynamic characteristics as functions of cut and patch locations, length and the number of treated and untreated segments has been done, theoretically.

v. An optimization procedure is given to determine the optimal number of treated segments and simultaneously their locations in order to maximize the modal damping factor corresponding to the first vibration mode for different end conditions.

vi. A finite difference model is developed to investigate the temperature gradient resulted over the time in the viscoelastic layer by the internal heat generation and examined its effect on the steady-state harmonic transverse response with time.

5.2 Major Conclusions

The major conclusions drawn from this research are summarized below:

i. The variations in the natural frequencies and the loss factors depend strongly on the thickness of the viscoelastic core layer. The natural frequencies corresponding to all the considered vibration modes decreases with an increase in the viscoelastic layer thickness, while the loss factors are increased for all modes.

ii. The nonlinear assumption in the displacement field of viscoelastic layer gives lower values of natural frequency and higher values of loss factor rather than for linear assumption of displacement field in viscoelastic core layer.

iii. The nonlinear assumption in the viscoelastic core layer presents more accurate results, whenever the ratio of the viscoelastic layer with the elastic base layer exceeds a certain value. The variations between two displacement theories become wider at higher range of frequencies.

iv. Partial-treatments of structures offer added design flexibility. Apart from the natural frequencies, the modal loss factors of the partially-treated viscoelastic sandwich beam could be controlled by placing both the treated and untreated segments within the beam span, irrespective of the boundary conditions.

v. Optimized partially treated clamped-clamped sandwich beam offer higher damping value than fully treated sandwich beam thus leads to the reduction in the weight of the structure.

vi.   Internal generated heat in viscoelastic layer, subjected to under harmonic load, leads to the development of temperature gradient in the core layer and thus would affect the damping properties of the viscoelastic material.

vii.   The variations in the damping properties of viscoelastic layer leads into the augmented steady-state harmonic response over a period of time.

5.3   Future Recommendations

In the present dissertation, the main parameters contributing to the damping behavior of the sandwich beam structure are investigated. Additional efforts may be required to extend the present analysis further as listed in the following:

i.   The developed finite element model can be further enhanced to consider the vibration damping analysis of both the sandwich plate and shell structures.

ii.   The optimization problem in partially treated sandwich beam can be solved to find the optimum damping for the higher modes.

iii.   The damping can be controlled using the standard control methodology to reduce the environmental disturbances such as the ambient temperature.

iv.   Effects of the heat dissipation can be formulated by considering the heat conduction in the lateral direction. Considering this problem, the heat transfer equation should be solved using the finite difference method for three dimensional irregular grids.

Bibliography

Baber TT, Maddox R.A and Orozco C.E. A fininte element model for harmonically excited viscoelastic sandwich beams [Journal] // Computers & Structures. - 1998. - 1 : Vol. 66. - pp. 105-113.

Bagley R.L. and Torvik P.J. Fraction Calculus - A Different Approach to Analysis of Viscoelastically Damped Strucutres [Journal] // AIAA Journal. - 1983. - 5 : Vol. 21. - pp. 741-748.

Bai J.M. and Sun C.T. The effect of viscoelastic adhesive layers on structural damping of sandwich beams. [Journal] // Mech.Struct. & Mach.. - 1995. - 1 : Vol. 23. - pp. 1-16.

Bishop R.E.D. The treatment of Damping Forces in Vibration Theory [Journal] // Journal of Royal Aeronautical Society. - 1955. - Vol. 59. - pp. 739-742.

Chen Q and Chan Y.W. Integral finite element method for dynamical analysis of elastic±viscoelastic composite structures [Journal] // Computers and Structures. - 2000. - Vol. 74. - pp. 51-64.

Christensen R M Theory of Viscoelasticity: An Introduction [Book]. - [s.l.] : New York Academic Press, 1971.

DiTaranto R A Theory of vibratory ending for elastic and viscoelasic layered finite-length beams. [Journal] // ASME Journal of applied mechanics. . - 1965. - Vol. 32. - pp. 881-886.

Ferry J.D. Viscoelastic Properties of Polymers [Book]. - New York : Wiley, 1980.

Golla D.F. and Hughes P.C. Dynamics of Viscoelastic strucutres- A Time Domain Finite Element Formulation [Journal] // Journal of Applied Mechanics. - 1985. - Vol. 52. - pp. 897-906.

Grootenhuis P The control of vibration with viscoelastic materials [Journal] // J.Sound.Vib. - 1970. - 4 : Vol. 11. - pp. 421-433.

Johnson C.D., Kienholz D.A. and Rogers L.C. Finite element prediction of damping in beams with constrained viscoelastic layers [Journal] // Shock and Vibration Bulletin. - 1981. - 1 : Vol. 51. - pp. 71-81.

Jones D. A Reduced-temperature Nomogram for Characterization of Damping Material Behavior [Journal] // Shock Vibration Bulletin. - 1978. - Vol. 48. - pp. 1-11.

Jones D. Handbook of Viscoelastic Vibration Damping [Book]. - [s.l.] : John Wiley & Sons, 2001.

Jones D. On temperature-frequency analysis of polymer dynamic mechanical behaviour. [Journal] // Journal of Sound and Vibration. - 1990. - Vol. 140. - pp. 85-102.

Kerwin E.M. Damping of flexural waves by a constrained viscoelastic layer. [Journal] // Journal of the Acoustical Society of America. - 1959. - Vol. 31. - pp. 952-962.

Kung S.W. and Singh R. Development of approximate methods for the analysis of patch damping design concepts. [Journal] // Journal of Sound and Vibration.. - 1999. - Vol. 219. - pp. 785-812.

Lall A.K, Asnani N.T. and Nakra B.C. Damping analysis of partially covered sandwich beams [Journal] // Journal of Sound and Vibration.. - 1988. - Vol. 123. - pp. 247-259.

Lall AK, Asnani NT and BC Nakra Vibration and damping analysis of rectangular plate with partially covered constrained viscoelastic layer. [Journal] // Journal of Vibration, Acoustics, Stress, and Reliability in Design.. - 1987. - Vol. 109. - pp. 241-247.

Leibowitz M. and Lifshitz J.M. Experimental Verification of Modal Parameters for 3-Layered Sandwich Beams [Journal] // Int. J. Solids Strucutres. - 1990. - 2 : Vol. 26. - pp. 175-184.

Lesieutre G. and Bianchini E Time Domain Modeling of Linear Viscoelasticity Using Anelastic Displacement Fields [Journal] // ASME Journal of Vibration and Acoustics. - 1995. - Vol. 117. - pp. 424-430.

Lesiutre G.A. and Mingori D.L. Finite Element Modeling of Frequency depedent Material Damping Using Augmenting Thermodynamics Fields [Journal] // J. Guidance and Control. - 1990. - 6 : Vol. 13. - pp. 1040-1050.

Lifshitz J.M. and Leibowitz M. Optimal sandwich beam design for maximum viscoelastic damping. [Journal] // Int. J. Solid Strucutres. - 1987. - Vol. 23. - pp. 1027-1034.

Mace M Damping of beam vibrations by means of a thin constrained viscoelastic layer: Evaluation of new theory [Journal] // Journal of Sound and Vibration. - 1994. - 5 : Vol. 172. - pp. 577-591.

McTavish D.J. and Hughes P.C. Modeling of linear viscoelastic space strucutres [Journal] // Journal of Vibration and Acoustics. - 1993. - Vol. 115. - pp. 103-110.

Mead D.J. A comparision of some equations for the flexural vibration of damped sandwich beams. [Journal] // Journal of Sound and Vibration.. - 1983. - 3 : Vol. 83. - pp. 363-377.

Mead D.J. and Markus S. The forced vibration of a three-layer damped sandwich beam with arbitarary boundary conditions. [Journal] // Journal of Sound and Vibration. - 1969. - 2 : Vol. 10. - pp. 163-175.

Muc A. and Gurba W. Genetic algorithms and finite element analysis in optimization of composite structures [Journal] // Composite Structures. - 2001. - Vol. 54. - pp. 275-281.

Nashif Ahid, D., Jones David, I.G. and Henderson John, P. Vibration Damping [Book]. - [s.l.] : John Wiley & Sons, 1985.

Nokes D.S. and Nelson F.C. Constrained layer damping with partial coverage [Journal] // Shock Vibration Bull. - 1968. - Vol. 38. - pp. 5-10.

Shaw Montgomery T. and MacKnight William J. Introduction to Polymer Viscoelasticity [Book]. - New Jersey : John Wiley & Sons, 2005.

Soni M.L. Finite element analysis of viscoelastically damped sandwich structures [Journal] // Shock and Vibration Bulletin. - 1981. - 1 : Vol. 51. - pp. 97-109.

Soong T.T. and Dargush G.F. Passive Energy Dissipation Systems in Strucutral Enginerring [Book]. - [s.l.] : John Wiley & Sons, 1997.

Ungar E.E. and Kerwin E.M. Jr Loss Factor of Viscoelastic Systems in terms of Energy Concepts [Journal] // Journal of the Acoustic Society of America. - 1962. - 7 : Vol. 34. - pp. 954-957.

Yan M.J. and Dowell E.H. Governing equations for the measurement of damping sandwich plates and beams. [Journal] // ASME Journal of Applied Mechancis.. - 1972. - Vol. 94. - pp. 1041-1047.

Zener Clarence Elasticity and Anelasticity of metals [Book]. - Chicago : The University of Chicago Press, 1948.

Appendix A

The detailed expression for the coefficients of the assumed polynomial series in Eq. (2.56) discussed in section 2.4.2 are given here.

$$a_0 = -\left(\frac{2u_b^2 - 2u_t^2 + H_b\theta_b^2 + H_t\theta_b^2 + H_t\theta_t^2 + H_v\theta_t^2}{2eH_v}\right)$$

$$-\left(\frac{H_v\left(2u_b^1 - 4u_b^2 + 2u_b^3 - 2u_t^1 + 4u_t^2 - 2u_t^3 + H_b\theta_b^1 - 2H_b\theta_b^2 + H_b\theta_b^3 + H_t\theta_b^1 - 2H_t\theta_b^2\right)}{6L^2e^2}\right) \quad \text{(A.1)}$$

$$-\left(\frac{H_v\left(H_t\theta_b^3 - H_t\theta_t^1 - 2H_t\theta_t^2 + H_t\theta_t^3 - H_v\theta_t^1 - 2H_v\theta_t^2 + H_v\theta_t^3\right)}{6L^2e^2}\right)$$

$$a_1 = \left(\frac{\theta_t^1 - \theta_t^3}{2Le}\right) + \left(\frac{2u_b^1 - 2u_b^3 - 2u_t^1 + 2u_t^3 + H_b\theta_b^1 - H_b\theta_b^3 + H_t\theta_b^1 - H_t\theta_b^3 + H_t\theta_t^1 - H_t\theta_t^3}{2H_vLe}\right) \quad \text{(A.2)}$$

$$a_2 = -\left(\frac{\theta_t^1 - 2\theta_t^2 + \theta_t^3}{L^2e}\right) - \left(\frac{2u_b^1 - 4u_b^2 + 2u_b^3 - 2u_t^1 + 4u_t^2 - 2u_t^3}{H_vL^2e}\right)$$

$$-\left(\frac{H_b\theta_b^1 - 2H_b\theta_b^2 + H_b\theta_b^3 + H_t\theta_b^1 - 2H_t\theta_b^2 + H_t\theta_b^3 - 2H_t\theta_t^1 + H_t\theta_t^3}{H_vL^2e}\right) \quad \text{(A.3)}$$

Appendix B

The detailed discussion on heat flow rate, presented in section 4.3, is described.
According to the Fourier law of heat conduction the rate of heat flow between the
node N and the adjacent node P is calculated as

$$Q_{NP} = k_{NP} A_{NP} \frac{T_N - T_P}{L_{NP}}$$
(B.1)

where kNP is the thermal conductivity , A_{NP} is the area normal to the direction of
heat flow between N and P, L_{NP} is the distance between the two nodes N and P and
T_N and T_P are the nodal temperatures. The control volume can then be measured as

$$V = \frac{1}{2}(S_N + S_N)\Delta.\frac{1}{2}(S_E + S_W)\Delta.\frac{1}{2}(S_I + S_O)\Delta$$
(B.2)

The area normal to the direction of the heat flow between N and P is given by

$$A_{NP} = \frac{1}{2}(S_E + S_W)\Delta.\frac{1}{2}(S_I + S_O)\Delta$$
(B.3)

Which can be simplified, by using Eq. (B.3), to the following expression

$$A_{NP} = \frac{V}{\frac{\Delta}{2}(S_N + S_S)}$$
(B.4)

The distance between the nodal point N and P is represented by the non-
dimensional term according to the reference value Δ is

$$L_{NP} = S_N \Delta$$
(B.5)

From the above, the heat flow rate from N to P can be written as

$$Q_{NP} = k_{NP} \frac{V}{\frac{\Delta}{2}(S_N + S_S)} \frac{T_N - T_P}{S_N \Delta} \tag{B.6}$$

Similarly, rate of heat flow between other nodes can be formulated